


## Volatile element signatures in the mantles of Earth, Moon, and Mars: Core formation fingerprints from Bi, Cd, In, and Sn

K. RIGHTER <sup>1\*</sup>, K. PANDO<sup>2</sup>, N. MARIN<sup>3</sup>, D. K. ROSS<sup>2,4</sup>, M. RIGHTER<sup>5</sup>, L. DANIELSON<sup>2</sup>, T. J. LAPEN<sup>5</sup>, and C. LEE<sup>6</sup>

<sup>1</sup>Mailcode XI2, NASA Johnson Space Center, Houston, Texas 77058, USA

<sup>2</sup>Jacobs JETS, NASA Johnson Space Center, Houston, Texas 77058, USA

<sup>3</sup>School of Earth and Space Exploration, Arizona State University, Tempe, Arizona 85287, USA

<sup>4</sup>NASA Johnson Space Center, University of Texas El Paso, Houston, Texas 77058, USA

<sup>5</sup>Department of Earth and Atmospheric Sciences, University of Houston, Houston, Texas 77204, USA

<sup>6</sup>Department of Earth Science, Rice University, Houston, Texas 77005, USA

\*Corresponding author. E-mail: kevin.righter-1@nasa.gov

(Received 19 April 2017; revision accepted 12 October 2017)

---

**Abstract**—Volatile element concentrations in planets are controlled by many factors such as precursor material composition, core formation, differentiation, magma ocean and magmatic degassing, and late accretionary processes. To better constrain the role of core formation, we report new experiments defining the effect of temperature, and metallic S and C content on the metal-silicate partition coefficient (or  $D(i)$  metal/silicate) of the volatile siderophile elements (VSE) Bi, Cd, In, and Sn. Additionally, the effect of pressure on metal-silicate partitioning between 1 and 3 GPa, and olivine-melt partitioning at 1 GPa have been studied for Bi, Cd, In, Sn, As, Sb, and Ge. Temperature clearly causes a decrease in  $D(i)$  metal/silicate for all elements. Sulfur and C have a large influence on activity coefficients in metallic Fe liquids, with C causing a decrease in  $D(i)$  metal/silicate, and S causing an increase. Pressure has only a small effect on  $D(\text{Cd})$ ,  $D(\text{In})$ , and  $D(\text{Ge})$  metal/silicate. Depletions of Bi, Cd, In, and Sn in the terrestrial and Martian mantles are consistent with high  $PT$  core formation and metal-silicate equilibrium at the high temperatures indicated by previous studies. A late Hadean matte would influence Bi the most, due to its high  $D$  (sulfide/silicate)  $\sim 2000$ , but segregation of a matte would only reduce the mantle Bi content by 50%; all other less chalcophile elements (e.g., Sn, In, and Cd) would be minimally affected. The lunar depletions of highly VSE require a combination of core formation and an additional depletion mechanism—most likely the Moon-forming giant impact, or lunar magma ocean degassing.

---

### INTRODUCTION

The origin of volatile elements in the Earth, Moon, and Mars is not well constrained; however, several theories have been proposed based on volatile elements such as In, As, Se, Te, and Zn, which are depleted in the Earth, Moon, and Mars relative to chondrites. Explanations for these low concentrations are based on two contrasting theories for the origin of Earth: equilibrium core formation versus late accretion. One idea is that the volatiles were added during growth of

the planets and Moon, and with halogens and lithophile elements remaining in the mantle, and the more siderophile elements mobilized into the metallic core (e.g., Righter et al. 2011) with a depletion commensurate with the magnitude of the metal/silicate partition coefficient,  $D(i)$  metal/silicate. A competing idea is that they were added to the mantles after core formation had completed (e.g., Albarede 2009). For many other refractory siderophile elements, the abundances in the mantle can be explained by high pressure and temperature ( $PT$ ) equilibrium between

molten mantle and metallic core (Wade and Wood 2005; Mann et al. 2009; Righter 2011; Siebert et al. 2013). Such a deep magma ocean scenario on the early Earth can account for moderately siderophile elements (Ni, Co, Mo, and W), weakly siderophile elements (Mn, V, Cr, and Nd), and some moderately volatile siderophile elements (VSE; Ge, Ga, Cu, and P). The highly volatile elements have yet to be tested for this scenario, primarily due to lack of experimental data at conditions required to evaluate this theory.

Bi, Cd, In, and Sn all display depletions in Earth's mantle relative to CI chondritic concentrations (Fig. 1). Cadmium isotopes have been measured in a wide variety of materials with an aim to constrain the volatile history of inner solar system material (e.g., Wombacher et al. 2003, 2008; Schediwy et al. 2006), and Cd distribution within the Earth's oceans and crust has been studied in detail as well (Horner et al. 2013; Hohl et al. 2017). However, a primary control on Cd distribution in the Earth's interior—core/mantle partitioning—is relatively poorly understood. The lower values of VSE in the terrestrial mantle could be caused by core formation, which would sequester siderophile elements into the core, or by volatility as Earth's building blocks may have been volatile element-depleted relative to CI chondrites. The terrestrial values could also be attributed to a combination of both core formation and volatility. Testing these ideas involves quantitative modeling which can only be performed after data are obtained on the systematic partitioning behavior of volatile elements with temperature, pressure, and melt composition. Such data for Bi, In, and Cd have been lacking, and the goal here was to study temperature and melt compositional effects to complement existing studies (Ballhaus et al. 2013; Wang et al. 2016; Righter et al. 2017a, 2017b). Combining our metal-silicate partition coefficient data for Bi, Cd, In, and Sn with published data will allow prediction of  $D$  and thus can be used to evaluate potential conditions under which terrestrial planets differentiated into core and mantle, and how they acquired volatiles.

## EXPERIMENTAL METHODS

Experiments were conducted at constant pressure and variable temperatures using a nonend-loaded piston cylinder apparatus with a type C W-Re thermocouple at NASA-JSC. The sample used for these experiments was a ground, mechanically mixed powder composed of 70 wt% Knippa basalt, the composition of which is described in Lewis et al. (1993); 24 wt% Fe; and 2 wt% each  $\text{Bi}_2\text{O}_3$ ,  $\text{In}_2\text{O}_3$ : $\text{SnO}_2$  (90:10 wt%), and Cd. Polycrystalline MgO and graphite were the two capsule

types used in an assembly with a  $\text{BaCO}_3$  pressure medium. Upon reaching a constant pressure of 1.0 GPa, samples were heated to silicate superliquidus temperatures for durations based on equilibration times from previous experiments (Li and Agee 1996; Righter and Drake 1997). Afterward, the samples were power quenched to glass or polyphase quench crystals surrounding large metallic liquid spheres.

Three different experiment series were performed with this composition, including a time series with graphite capsules (30, 60, 90, and 120 min), and two temperature series from 1500 to 1900 °C, each using different capsules (either MgO or graphite) for a total of 14 experiments. Two additional experiments at 1700 °C and MgO capsules included addition of FeS at 5% and 10% of the metal, and were designed to investigate the effect of sulfur alloyed in the metal.

A pressure series was carried out at 1, 2, and 3 GPa, all at 1900 °C, to investigate the effect of pressure on partition coefficients in a pressure range relevant to the lunar interior. These experiments utilized a bulk composition in the CaO-MgO-FeO-SiO<sub>2</sub>-Al<sub>2</sub>O<sub>3</sub> system with essentially no TiO<sub>2</sub>, K<sub>2</sub>O, Na<sub>2</sub>O, or P<sub>2</sub>O<sub>5</sub>. In addition to Bi, Cd, Sn, and In, we also added As, Ge, and Sb. The metallic portion was added in the same ratio (30:70) with silicate as above. Two experiments were carried out without metal, also at 1900 °C, and stabilized olivine. These were used to investigate the olivine-melt partitioning of these eight VSE.

Finally, to measure the effect of S and C on Bi, Cd, In, and Sn partitioning, we carried out several solid metal/liquid metal (SM/LM) experiments in the Fe-S and Fe-C systems, both at 1250 °C. These experiments were designed to examine the gross effects of each light element on the partitioning, especially as so little information exists for these elements. Compositions were targeted that had solid and liquid in the Fe-S and Fe-C systems at 1250 °C.

## ANALYTICAL METHODS

Samples were mounted in epoxy, sectioned, and polished, and then examined using either a JEOL LV5910 scanning electron microscope or JEOL 8530F field emission gun microprobe imaging at NASA-JSC (Fig. 2). The bright phases are spheres of metal that equilibrated with the silicate melt, which is darker. For experiments carried out with graphite capsules, all metals were carbon saturated. The metal and silicate samples were analyzed for major element composition using a Cameca SX100 and JEOL 8530 FEG-EMPA for electron microprobe analysis (EMPA) both at NASA-JSC. For metals, 15 kV accelerating voltage and

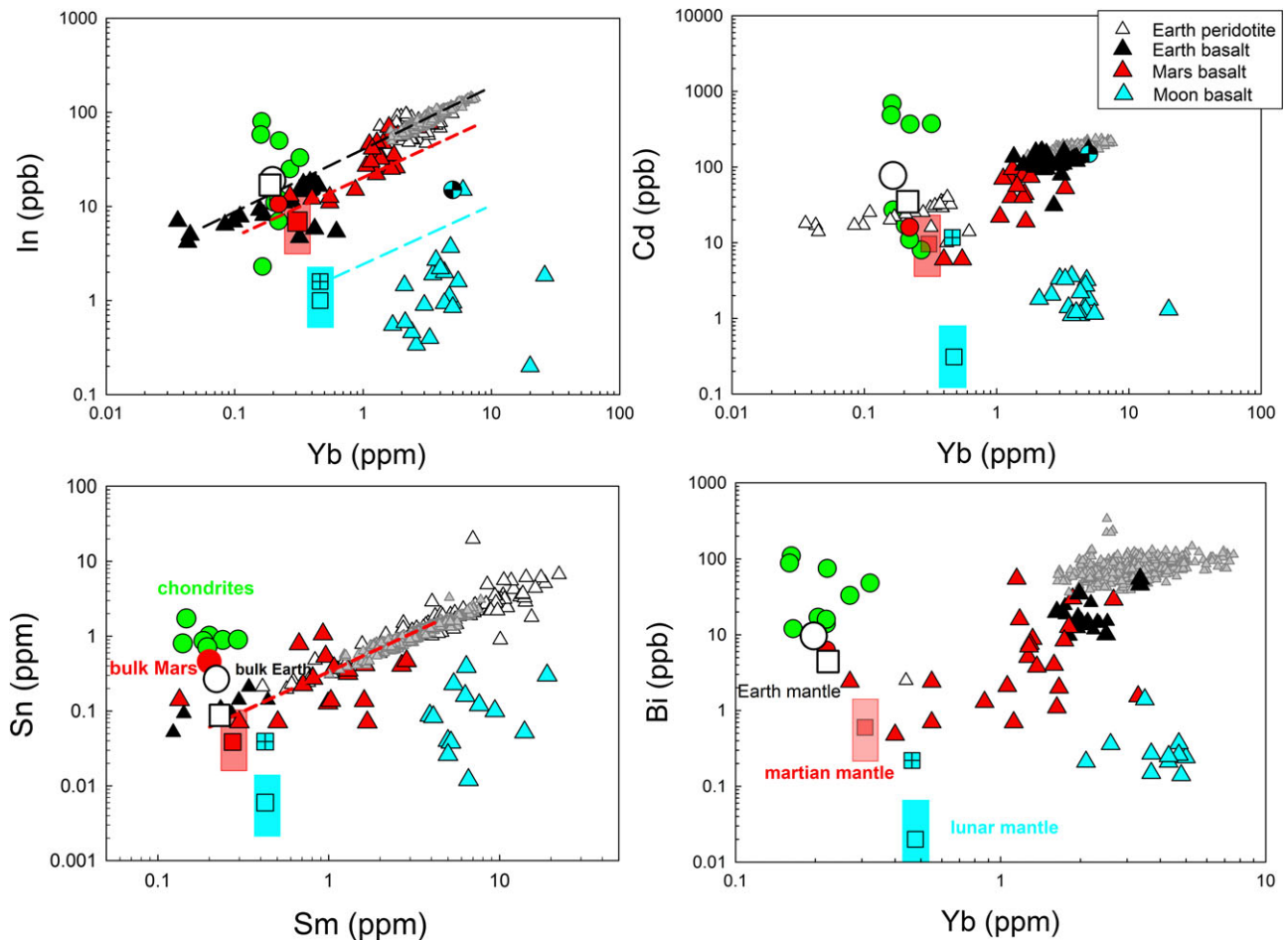


Fig. 1. Depletion diagrams for Bi, Cd, In, and Sn showing chondritic abundances (green circles) as well as terrestrial basalt and peridotite (black and open gray triangles), Martian basalt (red triangles), lunar basalt (blue triangles), lunar glass beads (black and blue circles for In and Cd only from Hauri et al. 2015), and estimates of the Martian and lunar mantles derived here and from the literature (large squares), as well as the uncertainty in those values (shaded blue and red for Moon and Mars mantles, respectively). Bulk Earth and Mars value are plotted as open and red circles, respectively (see Table 6 for all values). Bi, Cd, and In all share similar incompatibility with Yb, while Sn shares similar incompatibility with Sm. Indium and Cd in the Earth and Moon are higher than in some chondrites due to their volatile nature. Sources of terrestrial data—Hertogen et al. (1980), Jochum et al. (1993), Yi et al. (1995, 2000), Norman et al. (2004), Witt-Eickschen et al. (2009), Jenner et al. (2012), Jenner and O'Neill (2012), Jochum et al. (2016), and Hauri et al. (2015). Sources of Mars data—Laul et al. (1972), Burghele et al. (1984), Smith et al. (1984), Lodders (1998), Wang et al. (1999), Warren et al. (1999), and Yang et al. (2015). Sources of Moon data—Taylor et al. (1971), Wänke et al. (1970, 1971, 1972, 1973), Wolf et al. (1979), and BVSP (1981). All chondrites from the compilation of Newsom (1995).

30 nA sample current was used during analysis; for silicates (glasses and olivines), a sample current of 10 nA was used. For both the metal and the glasses with coarse-grained quench texture, a defocused 30  $\mu\text{m}$  beam was used for analysis, and typically 40–50 points were analyzed and averaged to obtain a representative composition of the metallic and silicate melts. A variety of natural and synthetic standards were used, e.g., Fe, Ni, Bi, Cd, InP, Sn, Fe<sub>3</sub>C, and FeS. Measurements of C in metal were acquired with a cold-finger chilled with liquid nitrogen, which strongly depresses C surface contamination. The JEOL 8530 microprobe is equipped

with oil-free scroll pumps, and turbo pumps rather than diffusion pumps, and these features minimize C contamination problems. To avoid interferences among the many Cd, In, and Sn L lines and by second- and third-order Fe K $\alpha$  and K $\beta$  peaks, backgrounds were set accordingly. Analyses are reported in Tables 1–5, and typically have  $2\sigma$  error  $\sim 2\%$ . In silicate-bearing samples, the Bi, Cd, In, and Sn content of the glass was lower than the detection limit of the EMPA; therefore, the silicate samples were also analyzed for trace element composition using laser ablation inductively coupled plasma-mass spectrometry (LA-ICP-MS) at Rice

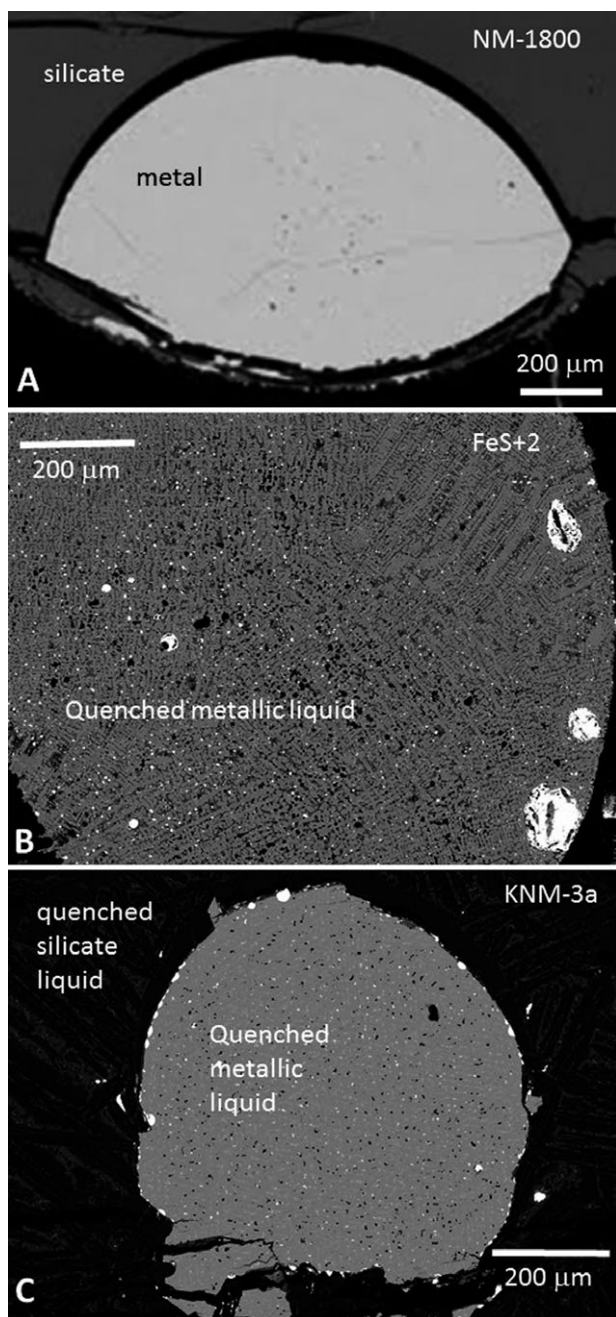


Fig. 2. A) Backscattered electron (BSE) image of sample NM-1800 run at 1800 °C and 1 GPa. The sample resulted in quenched metallic liquid (light gray) surrounded by silicate glass (dark gray) which is encased in the graphite capsule (black). B) Backscattered electron (BSE) image of sample FeS+2 run at 1700 °C and 1 GPa in an MgO capsule. The sample consists of quenched metallic liquid (intermediate gray) with blebs of Bi-rich metal near the edges of the metallic sphere. C) Backscattered electron (BSE) image of sample KNM-3a run at 1900 °C and 3 GPa in an MgO capsule. The sample consists of quenched metallic liquid (intermediate gray) and again with blebs of Bi-rich metal at the edges of the metallic sphere. Silicate melt appears dark in this image to highlight the contrast within the quenched metallic liquid.

University (using a similar approach to that of Righter et al. 2011). Standards used for the laser analysis were NIST610, NIST612, BHVO2g, and BCR2g glasses. Spot size varied from 50 to 200  $\mu\text{m}$  (30–40  $\mu\text{m}$  depth), depending on the size of the sample, but most spots were 200  $\mu\text{m}$  to maximize the area and volume being measured. Analysis was performed at low resolution (LR) and normalized to  $^{43}\text{Ca}$  isotope. The only trace elements specifically studied for this research were  $^{42}\text{Ca}$ ,  $^{43}\text{Ca}$ ,  $^{111}\text{Cd}$ ,  $^{110}\text{Cd}$ ,  $^{115}\text{In}$ ,  $^{117}\text{Sn}$ ,  $^{118}\text{Sn}$ ,  $^{119}\text{Sn}$ ,  $^{209}\text{Bi}$ ,  $^{69}\text{Ga}$ , and  $^{71}\text{Ga}$ . Data from the analysis of  $^{209}\text{Bi}$ ,  $^{111}\text{Cd}$ ,  $^{115}\text{In}$ , and  $^{119}\text{Sn}$  at LR were used to calculate Cd, In, Bi, and Sn in ppm in the silicates. Analyses are reported in Tables 1 and 2, along with  $2\sigma$  error, which is close to 10%.

Analyses of the KNM series experiments (KNM-1a, -2a, -3a, and -1 and -2) were performed at the University of Houston using a Photon Machines Analyte. 193 ArF laser ablation system coupled to a Varian 810-MS ICP-MS. During LA-ICP-MS, we measured  $^{25}\text{Mg}$ ,  $^{29}\text{Si}$ ,  $^{43}\text{Ca}$ ,  $^{72}\text{Ge}$ ,  $^{75}\text{As}$ ,  $^{111}\text{Cd}$ ,  $^{113}\text{In}$ ,  $^{115}\text{In}$ ,  $^{118}\text{Sn}$ ,  $^{121}\text{Sb}$ , and  $^{209}\text{Bi}$ . For the analysis of these experiments, we used a round  $\sim 60$   $\mu\text{m}$  diameter laser spot at the sample surface, a repetition rate of 8 Hz, and a laser power setting of  $2.99 \text{ J cm}^{-2}$ . The carrier gas used to carry ablated material to the detector was He at a flow rate of  $500 \text{ mL min}^{-1}$ . For each analyzed point, we measured a 20 s gas blank prior to sample ablation, followed by  $\sim 30$  s ablation on the sample. All trace element data were corrected for laser and ICP-MS elemental fractionation with NIST 612, and  $^{43}\text{Ca}$  as an internal standard. Data were reduced using the Glitter software (Van Achterbergh et al. 1999). Analyses are reported in Tables 3 and 4, along with  $2\sigma$  error. Previous studies by our group have demonstrated good agreement between the Rice and UH LA-ICP-MS instruments (Righter et al. 2017a, 2017b), and a comparison for Bi, Cd, In, and Sn is presented in Table S1 in supporting information.

## RESULTS

### Phase Relations and Equilibrium

All metal/silicate experiments contain metallic spheres that equilibrated with silicate melt, with one exception: M1500 contained SM, not LM, because its melting point is higher than 1500 °C. Upon quench, the metallic spheres form a quench texture comprised of multiple metallic phases that stabilize during cooling. Similarly, for the experiments in MgO capsules, the silicate melt does not quench to a glass but rather to a matte (or intergrown mixture) of glass and quench crystals, due to the reaction of the MgO capsule with

Table 1. Summary of all the metal-silicate experiments with MgO capsules (all at 1 GPa).

Sample	M1500	M1600	M1700	M1800	M1900	FeS+1	FeS+2
$T$ ( $^{\circ}\text{C}$ )	1500	1600	1700	1800	1900	1700	1700
Duration (min)	180	90	45	15	10	45	45
$\Delta\text{IW}$ (ideal)	-2.15 (3)	-2.25 (3)	-2.36 (3)	-2.41 (3)	-2.82 (3)	-2.35 (3)	-2.07 (3)
$\Delta\text{IW}$ (activity)	-1.75 (3)	-1.84 (3)	-1.95 (3)	-2.00 (3)	-2.41 (3)	-1.95 (3)	-1.66 (3)
<i>Silicate (EMPA)</i>							
$\text{SiO}_2$	29.8 (6)	28.8 (6)	31.7 (7)	31.9 (7)	32.6 (7)	31.9 (7)	32.3 (7)
$\text{TiO}_2$	4.29 (8)	3.92 (8)	2.62 (5)	2.55 (5)	3.08 (6)	2.55 (5)	2.64 (5)
$\text{Al}_2\text{O}_3$	9.57 (19)	11.49 (21)	8.31 (16)	7.84 (15)	9.22 (18)	8.56 (17)	8.07 (16)
$\text{Cr}_2\text{O}_3$	0.010 (1)	0.020 (1)	n.d.	0.010 (1)	0.010 (1)	n.d.	n.d.
$\text{FeO}$	14.7 (3)	13.0 (3)	11.6 (2)	11.1 (2)	8.70 (17)	10.68 (21)	11.47 (23)
$\text{MnO}$	0.160 (3)	0.160 (3)	0.130 (3)	0.130 (3)	0.110 (2)	0.120 (2)	0.130 (3)
$\text{MgO}$	16.5 (3)	21.1 (4)	31.6 (6)	32.1 (6)	29.2 (6)	34.3 (7)	29.6 (6)
$\text{CaO}$	15.0 (3)	13.7 (3)	8.46 (17)	9.00 (18)	11.3 (2)	7.99 (16)	9.51 (19)
$\text{Na}_2\text{O}$	3.98 (8)	3.59 (8)	2.07 (4)	1.99 (4)	2.92 (6)	2.06 (4)	3.44 (7)
$\text{K}_2\text{O}$	2.45 (4)	2.10 (4)	1.30 (3)	1.28 (2)	1.67 (3)	1.23 (2)	1.80 (4)
$\text{P}_2\text{O}_5$	1.06 (2)	0.83 (2)	0.55 (1)	0.49 (1)	0.36 (1)	0.40 (1)	0.55 (1)
$\text{SO}_2$	0.030 (1)	0.010 (1)	–	0.020 (1)	0.020 (1)	–	–
Total	97.53	98.77	98.40	98.39	99.20	99.69	99.52
<i>LA-ICP-MS</i>							
Bi ppm	3.0 (3)	7.0 (7)	10.2 (9)	13.0 (1.3)	63.5 (6.4)	22.5 (2.3)	13.5 (1.4)
In ppm	2800 (280)	2400 (240)	2080 (210)	2160 (220)	4230 (420)	1480 (150)	825 (83)
Cd ppm	1140 (114)	1345 (135)	1450 (145)	1270 (127)	2540 (254)	1220 (122)	1620 (162)
Sn ppm	147 (15)	71 (7)	41 (4)	49 (5)	117 (12)	51.8 (5.2)	31.6 (3.2)
<i>Metal (EMPA)</i>							
Si	n.d.	0.040 (2)	n.d.	0.020 (1)	0.020 (1)	n.d.	0.040 (2)
C	0.65	–	–	–	–	0.402	0.678
P	0.10 (1)	0.19 (1)	0.50 (3)	0.30 (2)	0.57 (3)	0.30 (2)	0.12 (1)
S	0.004 (1)	0.031 (1)	0.028 (1)	0.034 (1)	0.046 (1)	1.35 (3)	10.22 (50)
Fe	98.14 (1.96)	96.88 (1.93)	96.51 (1.93)	94.99 (1.91)	94.50 (1.89)	91.32 (1.83)	81.25 (1.62)
Cd	0.074 (2)	0.380 (8)	0.380 (8)	0.370 (7)	0.330 (7)	1.62 (3)	2.19 (4)
In	0.250 (5)	1.60 (3)	1.52 (3)	1.47 (3)	1.58 (3)	1.38 (3)	1.52 (3)
Sn	0.250 (5)	0.410 (8)	0.390 (8)	0.440 (9)	0.50 (1)	0.350 (7)	0.310 (6)
Bi	0.0002 (1)	0.062 (2)	0.092 (3)	0.051 (3)	0.129 (2)	1.62 (3)	1.33 (3)
Total	99.47	99.59	99.42	97.68	97.68	98.34	97.09
$D$ Cd	0.65 (9)	2.8 (4)	2.6 (4)	2.9 (4)	1.3 (2)	13.3 (2.0)	13.5 (2.0)
$D$ In	0.89 (13)	6.7 (1.0)	7.3 (1.1)	6.8 (1.0)	3.7 (0.6)	9.3 (1.4)	18.4 (2.8)
$D$ Sn	17.0 (2.6)	57.7 (8.7)	95.1 (14.2)	89.8 (13.5)	42.7 (6.4)	67.6 (10.1)	98.1 (12.7)
$D$ Bi	0.67 (10)	88.6 (13.2)	90.2 (13.5)	39.2 (8.9)	20.3 (3.0)	720 (108)	985 (148)
$\ln K_D$ Cd	-7.4 (0.6)	-6.1 (0.4)	-6.3 (0.4)	-6.2 (0.4)	-7.2 (0.6)	-4.7 (0.4)	-4.5 (0.4)
$\ln K_D$ In	-19.5 (1.6)	-16.0 (1.3)	-16.3 (1.3)	-16.5 (1.3)	-18.3 (1.4)	-16.2 (1.3)	-14.6 (1.2)
$\ln K_D$ Sn	-7.0 (0.6)	-6.5 (0.5)	-6.2 (0.5)	-5.7 (0.4)	-8.5 (0.7)	-5.9 (0.4)	-5.0 (0.4)
$\ln K_D$ Bi	-28.0 (2.1)	-17.8 (1.4)	-17.7 (1.4)	-19.3 (1.5)	-19.3 (1.5)	-12.8 (1.0)	-11.9 (1.0)

n.d. = "not detected."

the basaltic starting materials to form more MgO-rich liquids that are difficult to quench to a glass. Experiments in graphite capsules experienced no reactivity with the silicate melt, and so those experiments all contain homogeneous glass. Equilibrium olivine formed in a few experiments including the KNM-1 and KNM-2 experiments.

In nearly every experiment, Bi-rich blebs of metal are present at the edges of the larger metallic spheres, indicating that Bi saturated in the Fe liquids (Fig. 2B). Furthermore, the Bi levels measured in both the glass

and metal are lower than the levels added to the starting materials. This is consistent with Bi saturation in the experiments.

Several lines of evidence can be used to assess whether equilibrium was approached in these experiments. First, experiments TS30, TS60, KNM-1600, and TS-120 define a time series carried out at 30, 60, 90, and 120 min, respectively, at 1.0 GPa and 1600  $^{\circ}\text{C}$ . After 60 min, the  $D(i)$  metal/silicate do not change (within error of measurements) and the system has equilibrated (Fig. 3). Finally, the experiments

Table 2. Summary of all the metal-silicate experiments in graphite capsules (all at 1 GPa).

Sample	C1500	C1600	C1700	C1800	C1900	TS30	TS60	TS120
$T$ ( $^{\circ}\text{C}$ )	1500	1600	1700	1800	1900	1600	1600	1600
Duration (min)	180	90	45	15	10	30	60	120
$\Delta\text{IW}$ (ideal)	-2.01 (3)	-2.20 (3)	-2.07 (3)	-2.11 (3)	-2.25 (3)	-2.11 (3)	-2.09 (3)	-2.10 (3)
$\Delta\text{IW}$ (activity)	-1.28 (3)	-1.42 (3)	-1.32 (3)	-1.38 (3)	-1.47 (3)	-1.34 (3)	-1.32 (3)	-1.33 (3)
<i>Silicate (EMPA)</i>								
SiO <sub>2</sub>	38.1 (8)	38.5 (8)	38.4 (8)	38.8 (8)	38.5 (8)	37.8 (8)	38.5 (8)	38.2 (8)
TiO <sub>2</sub>	3.36 (7)	3.37 (7)	3.22 (6)	3.19 (6)	3.28 (6)	3.46 (7)	3.30 (7)	3.23 (6)
Al <sub>2</sub> O <sub>3</sub>	9.88 (20)	9.77 (20)	9.57 (19)	9.56 (19)	9.80 (20)	8.80 (18)	9.53 (20)	9.80 (20)
Cr <sub>2</sub> O <sub>3</sub>	0.06 (1)	0.06 (1)	0.06 (1)	–	0.08 (1)	0.08 (1)	0.06 (1)	0.07 (1)
FeO	18.03 (36)	17.91 (36)	17.09 (34)	17.74 (35)	17.57 (35)	18.13 (36)	17.73 (35)	17.76 (35)
MnO	0.20 (1)	0.20 (1)	0.21 (1)	0.19 (1)	0.19 (1)	0.20 (1)	0.20 (1)	0.19 (1)
MgO	12.4 (2)	13.0 (3)	13.7 (3)	13.4 (3)	13.3 (3)	15.4 (3)	13.8 (3)	13.0 (3)
CaO	11.36 (22)	11.16 (22)	11.02 (22)	10.69 (22)	11.02 (22)	11.16 (22)	11.17 (22)	11.10 (22)
Na <sub>2</sub> O	2.59 (5)	2.61 (5)	2.55 (5)	2.62 (5)	2.48 (5)	2.13 (4)	2.41 (5)	2.60 (5)
K <sub>2</sub> O	1.54 (3)	1.52 (3)	1.51 (3)	1.52 (3)	1.50 (3)	1.18 (2)	1.46 (3)	1.60 (3)
P <sub>2</sub> O <sub>5</sub>	0.75 (2)	0.75 (2)	0.79 (2)	0.63 (2)	0.83 (2)	0.66 (2)	0.67 (2)	0.77 (2)
SO <sub>2</sub>	0.020 (2)	0.030 (2)	0.020 (2)	–	0.030 (2)	–	–	–
Total	98.08	98.83	98.28	98.28	98.56	98.95	98.86	98.34
<i>LA-ICP-MS</i>								
Bi ppm	4.5 (4)	7.0 (7)	11.0 (1.1)	16.0 (1.6)	14.5 (1.5)	10.0 (1.0)	9.2 (9)	5.7 (6)
In ppm	5780 (580)	7475 (750)	5520 (550)	6430 (643)	8770 (877)	6520 (652)	6224 (620)	6500 (650)
Cd ppm	2910 (290)	5473 (550)	3500 (350)	3773 (380)	5270 (530)	3550 (360)	3200 (320)	3331 (330)
Sn ppm	237 (24)	312 (31)	273 (27)	274 (27)	360 (36)	261 (26)	245 (25)	273 (27)
<i>Metal (EMPA)</i>								
Si	n.d.	n.d.	n.d.	n.d.	n.d.	n.d.	n.d.	n.d.
C	5.59 (11)	6.04 (12)	5.91 (12)	6.09 (12)	6.07 (12)	5.67 (11)	5.73 (11)	5.96 (12)
P	0.031 (1)	0.041 (1)	0.091 (2)	0.145 (3)	0.174 (4)	0.0020 (1)	0.0030 (2)	0.054 (2)
S	0.0120 (1)	0.0190 (4)	0.0160 (3)	0.0170 (3)	0.0160 (3)	0.0040 (1)	0.0070 (2)	0.009 (1)
Fe	91.21 (1.82)	94.93 (1.90)	92.11 (1.80)	94.47 (1.88)	94.46 (1.67)	93.05 (1.86)	91.64 (1.84)	93.92 (1.88)
Cd	0.039 (1)	0.055 (1)	0.068 (1)	0.064 (1)	0.092 (2)	0.031 (1)	0.025 (1)	0.044 (1)
In	0.340 (7)	0.344 (7)	0.378 (8)	0.370 (8)	0.429 (8)	0.385 (8)	0.489 (9)	0.337 (7)
Sn	0.266 (5)	0.27 (5)	0.280 (6)	0.253 (5)	0.254 (5)	0.304 (6)	0.337 (7)	0.253 (5)
Bi	0.0127 (2)	0.0175 (3)	0.0138 (3)	0.0134 (3)	0.0254 (5)	0.083 (2)	0.0030 (1)	0.0070 (2)
Total	97.57	101.72	98.87	101.49	101.52	99.54	98.20	100.59
$D$ Cd	0.13 (2)	0.10 (2)	0.19 (3)	0.17 (3)	0.17 (3)	0.087 (13)	0.078 (12)	0.13 (5)
$D$ In	0.59 (9)	0.46 (7)	0.68 (10)	0.58 (9)	0.49 (7)	0.59 (9)	0.79 (12)	0.52 (8)
$D$ Sn	11.2 (1.7)	8.7 (1.3)	10.3 (1.5)	9.2 (1.4)	7.1 (1.1)	11.6 (1.7)	13.8 (2.1)	9.3 (1.4)
$D$ Bi	28.2 (4.2)	25.0 (3.8)	12.6 (1.9)	8.4 (1.2)	17.5 (2.6)	83 (12)	3.3 (5)	12.3 (1.8)
$\ln K_D$ Cd	-8.7 (0.6)	-9.0 (0.6)	-8.4 (0.6)	-8.6 (0.6)	-8.4 (0.6)	-9.2 (0.6)	-9.3 (0.6)	-8.8 (0.6)
$\ln K_D$ In	-19.3 (1.5)	-19.9 (1.5)	-19.2 (1.5)	-19.5 (1.5)	-19.6 (1.5)	-19.4 (1.5)	-18.8 (1.5)	-19.7 (1.5)
$\ln K_D$ Sn	-6.8 (0.5)	-7.2 (0.5)	-7.0 (0.5)	-7.1 (0.5)	-7.5 (0.5)	-6.9 (0.5)	-6.7 (0.5)	-7.1 (0.5)
$\ln K_D$ Bi	-19.8 (1.5)	-20.0 (1.5)	-20.7 (1.5)	-21.2 (1.5)	-20.0 (1.5)	-17.1 (1.4)	-23.6 (1.7)	-21.5 (1.5)

n.d. = "not detected."

reported here are similar to or longer than experiments for which time series have been done for slow diffusing elements such as Mo<sup>+</sup> and P<sup>5+</sup>, as well as Ga<sup>3+</sup> and Sn<sup>4+</sup> (Righter and Drake 2000; Righter et al. 2010). Second, if the reaction of metal with silicate did not reach completion or equilibrium, there will be variable silicate compositions according to the equilibrium  $2\text{Fe} + \text{Mg}_2\text{SiO}_4 + \text{O}_2 = 2\text{MgO} + \text{Fe}_2\text{SiO}_4$  and one might expect to find zoned metal or olivine. However, the olivines are not compositionally zoned, indicating

that equilibrium has been attained. Metals, although not expected to show zoning as they are simply Fe-Bi-Cd-Sn-In alloys, were also homogeneous.

Olivine crystallized in experiments KNM-1 and KNM-2 (with MgO capsules), and the composition of the olivine and coexisting melt can be used to assess whether equilibrium was approached in the experiments. Olivine-melt  $K_D$  are consistent with equilibrium: calculated Fo contents ( $X_{\text{Fo}}$ ) based on the olivine-melt  $K_D(\text{Mg-Fe})$  models of Snyder and Carmichael (1992)

Table 3. Summary of metal-silicate experiments with Bi, Cd, In, Sn, Ge, As, and Sb and variable pressure.

Sample	KNM-1a	KNM-2a	KNM-3a
$T$ (°C)	1900	1900	1900
Duration (min)	9	6	10
GPa	1	2	3
$\Delta IW$ (ideal)	-2.21 (3)	-2.14 (3)	-2.29 (3)
$\Delta IW$ (activity)	-1.81 (3)	-1.73 (3)	-1.88 (3)
<i>Silicate (EMPA)</i>			
SiO <sub>2</sub>	33.34 (67)	33.74 (68)	27.61 (52)
TiO <sub>2</sub>	0.010 (1)	0.010 (1)	0.010 (1)
Al <sub>2</sub> O <sub>3</sub>	7.30 (15)	4.91 (10)	10.88 (20)
FeO	13.54 (27)	17.32 (34)	14.31 (28)
MnO	0.010 (1)	0.020 (1)	0.010 (1)
MgO	42.17 (84)	39.24 (78)	40.62 (81)
CaO	5.03 (10)	6.13 (11)	7.14 (13)
Na <sub>2</sub> O	0.010 (1)	0.020 (1)	0.010 (1)
K <sub>2</sub> O	0.010 (1)	0.030 (1)	0.020 (1)
P <sub>2</sub> O <sub>5</sub>	0.020 (2)	0.100 (10)	0.040 (6)
Total	101.43	101.52	100.66
<i>LA-ICP-MS</i>			
Bi ppm	38.8 (3.8)	74.5 (13.4)	84.3 (16.9)
In ppm	912 (102)	1388 (272)	1440 (260)
Cd ppm	895 (92)	2415 (560)	2170 (860)
Sn ppm	0.23 (6)	0.42 (6)	0.50 (10)
As ppm	2.04 (38)	4.23 (87)	1.01 (60)
Sb ppm	11.1 (1.4)	42.5 (9.6)	9.7 (4.2)
Ge ppm	31.1 (3.8)	71.8 (12.9)	56.8 (12.7)
<i>Metal (EMPA)</i>			
Si	0.040 (1)	0.050 (1)	0.060 (2)
C	n.a.	n.a.	2.11
P	0.020 (1)	0.030 (2)	0.070 (2)
S	0.010 (1)	0.010 (1)	0.010 (1)
Fe	90.09 (1.80)	91.14 (1.82)	92.03 (1.84)
Cd	0.220 (4)	0.270 (5)	0.330 (6)
In	1.25 (3)	1.09 (3)	0.88 (2)
Sn	0.010 (1)	0.008 (1)	0.008 (1)
Bi	1.86 (4)	0.68 (2)	1.49 (4)
As	1.35 (4)	1.14 (3)	1.23 (3)
Sb	1.74 (4)	1.25 (3)	1.65 (4)
Ge	1.41 (4)	1.31 (4)	1.34 (4)
Total	98.00	97.25	101.21
$D$ Cd	2.5 (4)	1.1 (2)	1.5 (2)
$D$ In	13.7 (2.1)	7.9 (1.2)	6.1 (9)
$D$ Sn	435 (65)	190 (29)	160 (24)
$D$ Bi	479 (72)	91 (14)	177 (27)
$D$ As	6620 (980)	2700 (400)	12200 (1800)
$D$ Sb	1570 (240)	294 (44)	1700 (260)
$D$ Ge	450 (70)	182 (27)	236 (35)
$\ln K_D$ Cd	-15.1 (1.3)	-15.4 (1.3)	-16.2 (1.3)
$\ln K_D$ In	-12.3 (1.1)	-14.5 (1.2)	-13.5 (1.2)
$\ln K_D$ Sn	-6.1 (0.5)	-6.7 (0.5)	-6.5 (0.5)
$\ln K_D$ Bi	-3.6 (0.3)	-4.0 (0.3)	-4.5 (0.3)
$\ln K_D$ As	-14.4 (1.2)	-14.7 (1.2)	-15.1 (1.2)
$\ln K_D$ Sb	-8.6 (0.7)	-9.6 (0.8)	-8.1 (0.7)
$\ln K_D$ Ge	0.5 (1)	-0.7 (1)	0.7 (1)

n.a. = not analyzed.

and Gee and Sack (1988) are within 0.01 of the measured olivine composition for each run (Table 4).

The two SM/LM partitioning experiments yielded  $D$  SM/LM values for all four elements.  $D$ (SM/LM) are  $\ll 1$  for Sn, In, Cd, and Bi confirming their chalcophile behavior. In the Fe-C system, on the other hand,  $D$  (SM/LM) are  $> 1$  for Sn, In, and Cd; Bi exhibited slight preference for a C-bearing liquid over that of metal, with a  $D$ (SM/LM) = 0.7. The experiment in the Fe-C system also contained Fe carbide, thus allowing determination of  $D$ (FeCarbide/LM); none of these elements favor carbide, with Cd and Bi having  $D$  (FeCarbide/LM) of 0.57 and 0.46, respectively, and Sn and In  $< 0.1$  (Table 5).

### Oxygen Fugacity

Oxygen fugacity ( $fO_2$ ) is also necessary to quantify because metal-silicate partition coefficients can be sensitive to  $fO_2$  changes. Oxygen fugacity for each experiment was calculated relative to the IW buffer, using the relation  $\Delta IW = -2 \times \log(X_{Fe}/X_{FeO})$ , which is used in many studies of metal-silicate partitioning, and in this study ranged from 1.4 to 2.3  $\log fO_2$  units below the iron-wüstite buffer (Tables 1 and 2). For the regression calculations (see below), absolute  $fO_2$  is utilized, and calculated according to the relation  $\Delta IW = -2 \times \log(a_{Fe}/a_{FeO})$ , where  $fO_2$  for the IW buffer at  $P$  and  $T$  was calculated using the expression of Campbell et al. (2009), the activity of Fe in metal using the interaction parameter model of Righter et al. (2016), and the activity of FeO in the silicate melt from Holzheid et al. (1997). The KNM experiments designed to examine lunar interior pressure effects were at the low end of  $fO_2$  estimates for the Moon (IW-1 to IW-2; Sutton et al. 2005; Karner et al. 2006), and therefore highly relevant to understanding the Moon.

### Metal/Silicate Partition Coefficients

As observed in previous experimental studies (Righter et al. 2010, 2011), reaction of silicate melts with MgO capsules results in more MgO-rich silicate melts at higher temperatures. For these experiments, MgO varied from ~22 to ~32 wt% between 1600 and 1900 °C. The MgO capsule series discussion here excludes the 1500 °C experiment because the metal phase was solid, not liquid. Because some variation in  $D$ (metal/silicate) can be attributed to small differences in  $fO_2$ , we calculated the partition coefficients as an exchange coefficient with Fe based on the equilibrium:  $MO_{n/2}^{silicate} + (n/2)Fe^{metal} = M^{metal} + (n/2)FeO^{silicate}$ , where  $n$  is the valence of element  $M$  in the silicate melt. In this way, any effect due to  $fO_2$  can be avoided, and thus

Table 4. Summary of the olivine-melt experiments.

Sample	KNM-1 oliv	KNM-1 liq	$D$	KNM-2 oliv	KNM-2 liq	$D$
$T$ (°C)	1900			1900		
Duration (min)	10			10		
<i>EMPA</i>						
SiO <sub>2</sub>	39.86 (80)	38.01 (76)		41.45 (85)	37.05 (75)	
Al <sub>2</sub> O <sub>3</sub>	0.58 (1)	3.64 (7)		0.43 (1)	4.83 (8)	
FeO	2.50 (5)	4.09 (8)		1.69 (4)	5.12 (8)	
MgO	55.63 (1.11)	52.01 (1.04)		56.11 (1.08)	48.63 (99)	
CaO	0.29 (1)	0.68 (1)		0.32 (1)	3.42 (7)	
Na <sub>2</sub> O	0.010 (1)	0.010 (1)		0.020 (2)	0.020 (2)	
P <sub>2</sub> O <sub>5</sub>	0.010 (1)	0.030 (1)		0.010 (1)	0.030 (1)	
X <sub>Fo</sub>	0.98			0.98		
X <sub>Fo</sub> predicted <sup>a</sup>	0.99			0.99		
Total	98.88	98.47		100.04	99.14	
<i>LA-ICP-MS</i>						
Ge	5120 (175)	7600 (250)	0.68 (5)	5020 (350)	6930 (425)	0.73 (5)
As	190 (9)	5620 (246)	0.034 (3)	220 (30)	7450 (925)	0.030 (3)
Cd	570 (28)	3900 (177)	0.14 (2)	480 (50)	5140 (473)	0.094 (9)
In	1990 (69)	7600 (250)	0.26 (3)	1510 (130)	7340 (560)	0.21 (3)
Sn	0.21 (3)	0.94 (5)	0.22 (5)	0.15 (3)	0.62 (6)	0.25 (5)
Sb	148 (6)	6640 (250)	0.022 (3)	146 (16)	7900 (810)	0.019 (3)
Bi	41 (2)	7440 (347)	0.005 (1)	32 (2)	7040 (446)	0.005 (1)

<sup>a</sup>Forsterite content calculated using either the Gee and Sack (1988) and Snyder and Carmichael (1992) oliv-liq models.

Table 5. Composition of phases in the solid metal (SM)-liquid metal (LM), and iron carbide (FeCarb) partitioning experiments (EMPA).

Sample	Si	C	Fe	S	In	Sn	Cd	Bi	Total
Liq	0.056 (2)	2.10 (11)	62.28 (1.18)	33.0 (7)	0.68 (3)	0.06 (1)	1.84 (4)	0.88 (2)	100.89
Sol	0.007 (1)	0.88 (2)	96.01 (1.92)	0.07 (1)	0.0020 (1)	0.032 (1)	0.026 (1)	0.0030 (1)	97.03
$D(\text{SM/LM})$					0.0030	0.52	0.014	0.0034	
Liq	0.025 (1)	2.44 (15)	98.66 (1.97)	0.002	0.252 (5)	0.16 (1)	0.032 (2)	0.007 (1)	101.57
Sol	0.031 (1)	2.32 (13)	98.32 (1.97)	0.002	0.385 (7)	0.18 (1)	0.034 (2)	0.005 (1)	101.28
Carb	0.033 (1)	6.45 (31)	95.14 (1.90)	0.0019	0.0067 (1)	0.013 (1)	0.018 (1)	0.0032 (2)	101.66
$D(\text{SM/LM})$					1.53	1.13	1.06	0.71	
$D(\text{FeCarb/LM})$					0.03	0.08	0.57	0.46	

offers the best way to isolate a temperature effect. All four elements decrease over this temperature range, whether one considers  $\ln K_D$  or  $D(\text{metal/silicate})$  (Figs. 4A and 4B). The highest temperature experiments, at 1900 °C with MgO contents near 30 wt%, contain silicate melts with compositions closely approximating peridotite, and thus are highly relevant to core formation in a magma ocean setting for Earth.

In the temperature series carried out in graphite capsules, the silicate melt composition and pressure are fixed, and the metallic liquid composition is nearly constant with Fe-Bi-Cd-Sn-In-C alloys containing ~6 wt% C (Table 2). For this series, most exchange and partition coefficients decreased with temperature; those for Bi, Sn, and In all decrease with temperature while those for Cd stayed constant or increased slightly

(Figs. 4C and 4D). These experiments illustrate that  $D$  (metal/silicate) for all four elements decrease with C-saturation. Although these experiments are important for understanding the effects of compositional variation and dissolved C in metal, the MgO series is more relevant to Earth's peridotite mantle and low C core (e.g., Badro et al. 2015).

The pressure series of experiments (KNM) was designed to isolate any specific effect of pressure on  $D(i)$  metal-silicate. Across this modest pressure range, we did not observe significant variations (Fig. 5).  $D(\text{Ge})$ ,  $D(\text{Cd})$ ,  $D(\text{In})$ , and  $D(\text{Sn})$  metal/silicate all show a small decrease with pressure, whereas  $D(\text{As})$ ,  $D(\text{Sb})$ , and  $D(\text{Bi})$  metal/silicate have no obvious trend with pressure. These results are, in general, consistent with previous studies showing that pressure typically has a small or modest effect on partitioning (Righter 2015).



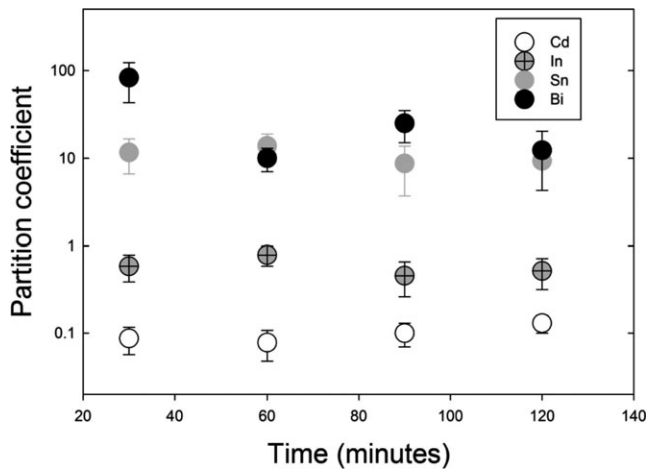


Fig. 3. Time series carried out at fixed temperature and pressure for 30, 60, 90, and 120 min. After 60 min, the  $D(i)$  metal/silicate do not change (within  $2\sigma$  error on measurements; Table 2) and the system has equilibrated.

The two experiments with variable S content of the metal reveal important effects of metallic sulfur content on all four elements.  $D(\text{Sn})$  and  $D(\text{In})$  metal/silicate exhibit a small or no effect of sulfur outside of known effects of  $f\text{O}_2$ , temperature, and melt composition (Figs. 4A and 4B).  $D(\text{Cd})$  and  $D(\text{Bi})$  metal/silicate, on the other hand, both exhibit significant increases with metallic S contents, demonstrating their chalcophile behavior. The same trends are evident whether one considers  $\ln K_D$  or  $D(\text{metal/silicate})$  partition coefficients (Figs. 4A and 4B). Bi and Cd should thus be sensitive indicators of chalcophile behavior—at least during core formation—as compared with In and Sn.

### Olivine/Melt Partition Coefficients

Although it is generally assumed that Bi, In, Cd, As, Sb, Ge, and Sn are incompatible during mantle melting, based on limited work in basaltic systems (Suzuki and Akaogi 1995; Righter and Drake 2000; Adam and Green 2006; Righter et al. 2009), there have not been focused studies on all these elements simultaneously. Here we systematically look at all, compare to previous measurements, and show that the low  $D(\text{Cd})$  and  $D(\text{Ge})$  olivine/silicate melt are consistent with Onuma-type diagrams for other 2+ cations (Mg, Fe, Ni, Mn, and Ca) (Fig. 6). We also show that the range of values measured here for  $D(\text{In})$ ,  $D(\text{Sb})$ ,  $D(\text{As})$ , and  $D(\text{Bi})$  olivine/silicate melt are consistent with trends observed for other 3+ cations such as Al, V, Sc, and Tm (Fig. 6).  $D(\text{Sb})$  olivine/silicate melt is lower than expected given its ionic radius, but this could be due to differing effects of nearest neighbor cations in the M1 and M2 sites of the olivine (e.g., Redfern et al. 2000).

The trends observed in all of these new series will be quantified using metal-silicate partitioning expressions derived below and combining our new data with literature data.

## DISCUSSION

### Depletions of Bi, Cd, In, and Sn in Earth, Moon, and Mars

Most siderophile element concentrations in planetary mantles are much lower than those measured in chondrites, and this has been attributed to several processes: volatile depletions in Earth's building blocks (Drake et al. 1989), segregation into the Earth's metallic core (Wänke and Dreibus 1986), mantle melting and sequestration in sulfide (Norman et al. 2004), and then later volatility due to giant impacts, magma ocean degassing, or later magmatism (Meyer et al. 1975).

### Processes Responsible for Depletions

**Precursor Volatile Depletions:** Earth's building blocks are known to have experienced volatility that ultimately dates back to nebular processes where partial condensation from nebular gas resulted in depletions of most volatile elements. The volatility trend is well defined by many lithophile volatile elements such as Na, K, Li, and Rb. The degree of volatility is usually quantified by 50% condensation temperature. Below values near 1200 K, elements exhibit larger and larger depletions due to volatility such that at temperatures as low as 300 K, depletion due to volatility could cause values  $100\times$  lower than that measured in chondrites. The degree of volatility might also be defined by melt-vapor equilibrium at higher temperatures relevant to melting and differentiation in precursor bodies (Norris and Wood 2017).

**Core Formation:** Many volatile elements are also siderophile and thus can be concentrated in the metal phase such as a metallic core. The volatility trend defined by lithophile elements can be used to estimate the degree to which the VSE were depleted before core formation processes. Once this estimate is made, the remaining (if any) depletion could be attributed to segregation into a Fe metallic core.

**Mantle Melting:** Most of the VSE—and specifically those studied here (Bi, Cd, In, and Sn)—are incompatible during melting of the mantle. Therefore, if a mantle VSE content has been set by precursor volatile element depletion and later core formation, and is then melted, the melts generated will have higher VSE content than the mantle due to incompatibility. As a result, if a VSE is plotted against a refractory lithophile element (RLE) of similar incompatibility, the two

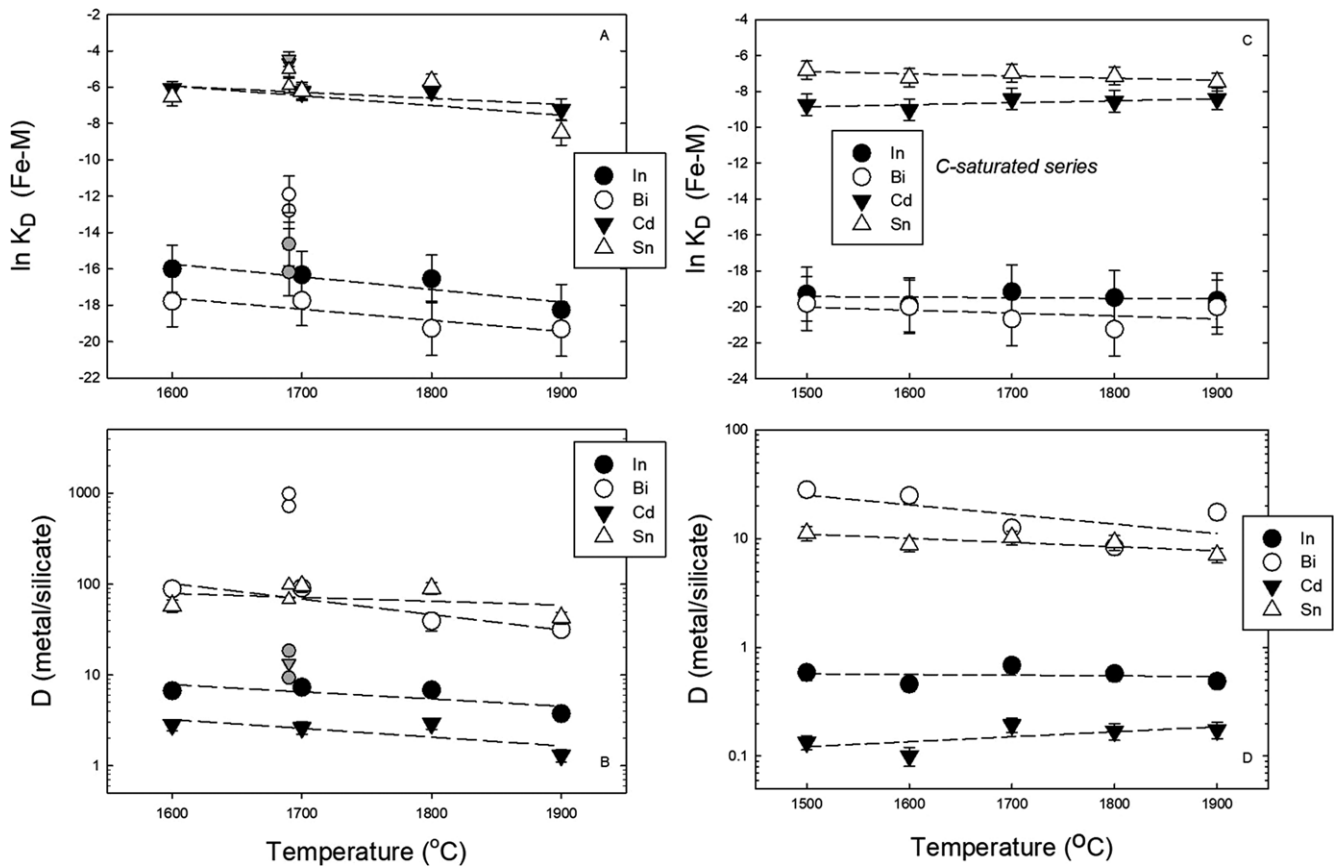


Fig. 4. A, B) Effect of temperature for Bi, Cd, In, and Sn utilizing both (A) the exchange coefficient  $\ln K_D$  or (B) the partition coefficient  $D$ (metal/silicate) for the MgO capsule series. Also shown are the two 1700 °C experiments with higher metallic S contents; these are plotted at 1690 °C for clarity and to avoid overlapping symbols. The effect of S is strong for Bi and Cd, but small to negligible for In and Sn. C, D) Effect of temperature for Bi, Cd, In, and Sn utilizing both (C) the exchange coefficient  $\ln K_D$  or (D) the partition coefficient  $D$ (metal/silicate) for the graphite capsule series (C-saturated). Most elements show a decrease in both coefficients with increasing temperature, but Cd shows a slight increase. Data and associated error are from Tables 1 and 2.

elements will define a 1:1 linear trend (e.g., Wänke and Dreibus 1986). Such examples can be seen in Sn-Sm, Cd-Yb, In-Yb, or Bi-Yb diagrams (Fig. 1), as well as in other siderophile-RLE pairs such as P-Nd, Mo-Pr, or W-U (e.g., Wänke and Dreibus 1986). The linear trend, coupled with an estimate of the RLE content of a mantle, can be used to estimate the VSE content of the mantle before melting. Deviations from a linear trend may occur if another process occurs which can fractionate the VSE but not the RLE. Two such processes are magmatic degassing or retention in sulfide.

**Sulfide Retention:** Chalcophile elements are strongly affected by the presence of sulfide. If a silicate melt becomes sulfide saturated, the sulfide will concentrate chalcophile elements and cause substantial reduction of chalcophile elements in the silicate melt (e.g., Righter et al. 2008a). Recent studies by Kiseeva and Wood (2013) and Li and Audétat (2015) demonstrate the magnitude of sulfide liquid/silicate liquid partition

coefficients for a wide range of chalcophile elements, with Bi, Cu, and Ni having the highest partition coefficients; Cd, Pb, and Co intermediate; and As, Mo, Sn, and Sb relatively low.

**Magmatic and Magma Ocean Degassing:** A potential mechanism for volatile loss on any differentiated body with a magma ocean stage (proposed for Earth, Moon, and Mars) is degassing of the magma ocean, or a large magma body, which can affect many elements. For example, the high  $\delta^{37}\text{Cl}$  measured in some urKREEP lunar samples suggests an important role for metal-chloride degassing (Barnes et al. 2016). Similarly, high  $\delta\text{D}$  and  $\delta^{52}\text{Zn}$  values for lunar materials suggest degassing played a role in generating these fractionated values (Paniello et al. 2012; McCubbin et al. 2015). Because the VSE are volatile by definition, they may be affected by degassing processes; degassing potential is gauged by emanation coefficients, which are known to be high for Re, Cd,

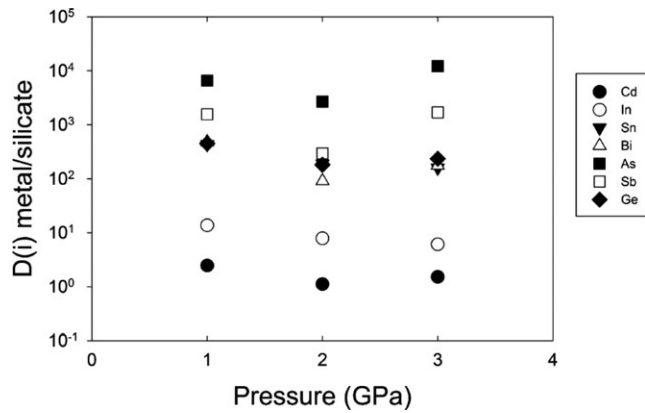


Fig. 5. Effect of pressure on  $D(i)$  metal/silicate for eight volatile siderophile elements.  $D(\text{Cd})$  and  $D(\text{In})$  metal/silicate both show a slight decrease with pressure, but most elements show no distinct trend within error of the partition coefficient measurement. Error bars are in most cases smaller than the symbol size.

and Bi, for example. It is well known from studies of trace metals in volcanic gases that many VSE can be concentrated in the gas phase (Rubin 1997; Norman et al. 2004), with Bi and Cd being strongly concentrated (emanation coefficients of 0.31 and 0.26, respectively), and Sn and In being less strongly but nonetheless high (emanation coefficients of 0.0012 and 0.0018, respectively). The relative volatilities of these elements were also confirmed by experiments of Norris and Wood (2017) at the low oxygen fugacities relevant to melting and differentiation in precursor bodies and protoplanets. Even the refractory element Re can be volatile at oxidizing conditions; Norman et al. (2004) suggested that Cd/Dy and Re/Yb ratios plotted against S content reveal significant magmatic degassing of Re and Cd (and also Bi) in a suite of Hawaiian glasses (Fig. 7). However, consideration of the extensive data set of Jenner et al. (2012) for mid-ocean ridge basalt (MORB) glasses of variable S content and degassing history reveals very limited degassing of these elements (Fig. 7). Degassing might account for concentration drops of  $2\times$  to  $3\times$  in Cd and Bi contents. In and Sn, on the other hand, show no evidence for degassing in the Jenner et al. (2012) MORB suite, and show entire overlap in Sn-Sm trends that are measured in subaerial terrestrial lavas (Fig. 7).

If a VSE were to be lost to a gas phase, it must also be mobile in magmas. Diffusion studies of As, Sb, Cd, Bi, and Pb have been carried out by MacKenzie and Canil (2008) and Johnson and Canil (2011), and all five of these elements have high diffusion coefficients that would allow mobility under magmatic conditions. However, detailed knowledge of many elements is lacking and the relative potential for degassing (such as emanation coefficients) is difficult to evaluate for all elements considered here. These observations will be

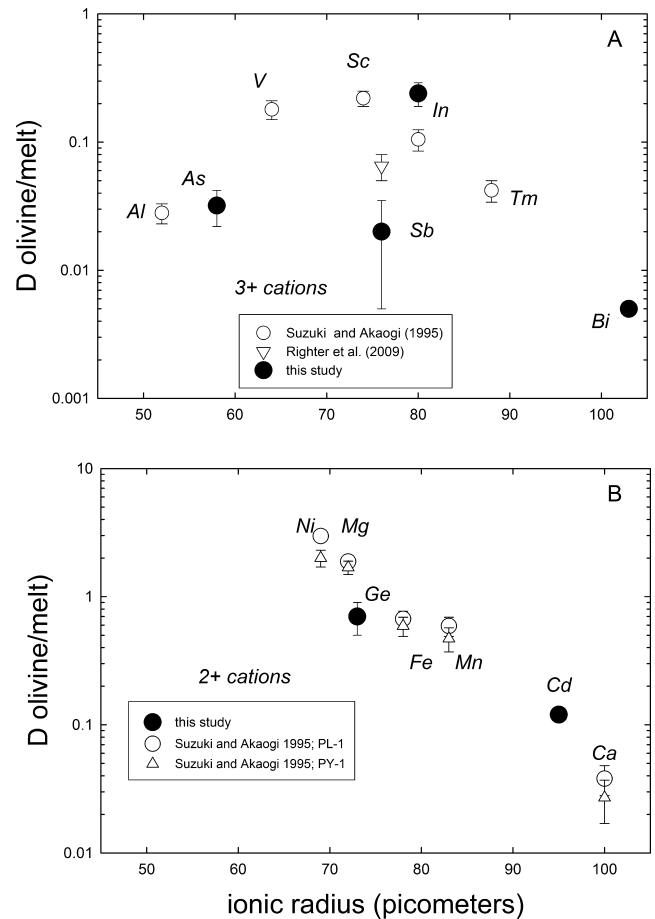


Fig. 6. A) Onuma diagrams for olivine/melt partitioning results for 3+ cations (As, In, Sb, and Bi) from this study, and for those from Suzuki and Akaogi (1995) for Al, V, Sc, In, and Tm, and Righter et al. (2009) for Sb. B) Onuma diagrams for olivine/melt partitioning results for 2+ cations (Ge and Cd) from this study, and for those from Suzuki and Akaogi (1995) for Ni, Mg, Fe, Mn, and Ca (for samples PL-1 and PY-1).

applied to lunar and Martian basalt data in the Earth section below.

The role of all these processes—precursor volatility, core formation, sulfide segregation, and magmatic volatility—must be assessed so that their effect on VSE concentrations in Martian, lunar, or terrestrial basalt can be interpreted. If a solid understanding exists of these processes then mantle concentrations of VSE in the Moon and Mars can be estimated using knowledge of the geochemical behavior. Correlations between Bi-Yb, Cd-Yb, In-Yb, Sn-Sm (VSE-RLE pairs) define VSE depletions in Earth, Moon, and Mars, as we will see in the discussions below.

### Earth Mantle

Earth mantle concentrations of Bi, Cd, Sn, and In are known from studies of mantle xenoliths and massifs.

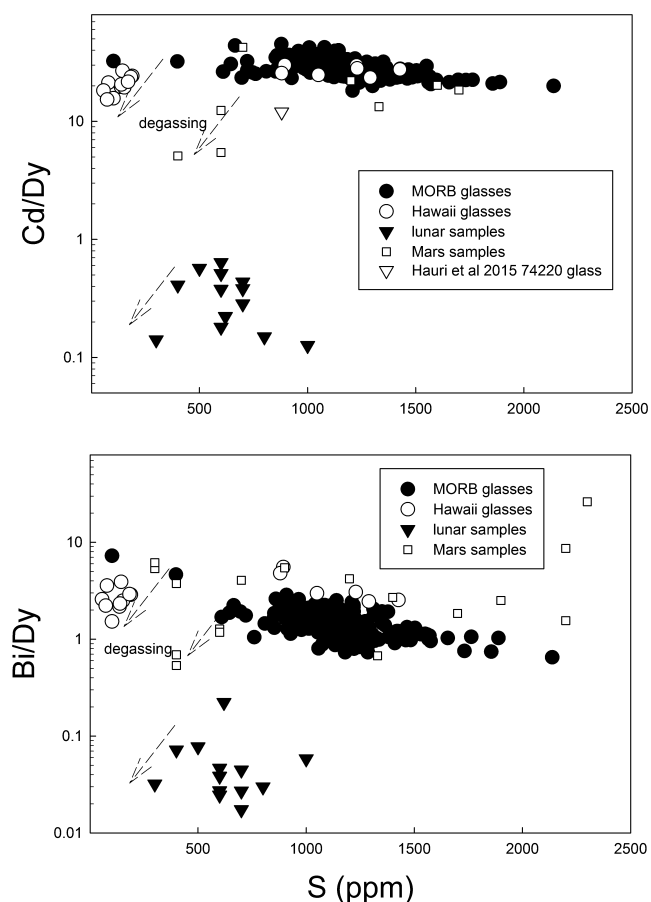


Fig. 7. Cd/Dy and Bi/Dy versus S for MORB glasses (Jenner et al. 2012), Hawai'i glasses (Norman et al. 2004), lunar basalts (Wolf et al. 1979), and Martian meteorites (Yang et al. 2015). Lunar glass bead of Hauri et al. (2015) is only available for Cd/Dy versus S. Norman et al. (2004) identified degassing trends shown for the lowest S samples in the Hawai'i suite. Such behavior may be evident in the lunar and Martian samples and thus may place limits on the extent of degassing. The large extent of degassing implied by the Hauri et al. (2015) reconstructed glass analysis seems at odds with the other data for the Moon, and data for Earth and Mars.

The concentrations in Earth's primitive upper mantle were most recently reviewed by Palme and O'Neill (2014).

#### Moon Mantle

Because degassing has been proposed for many lunar basalt suites, lunar basalts could represent degassed magmas and thus undegassed mantle melts might have higher Cd and Bi than what is measured in surficial eruptive units. Examination of Cd/Dy and Bi/Dy versus S (suggested by Norman et al. [2004] as an indicator of extent of degassing) shows that lunar basalts with the lowest S contents may have degassed Cd and Bi by a factor of 5 from those at intermediate S

contents. The intermediate to high S content glasses actually show a slight increase in Cd/Dy and Bi/Dy with decreasing S content as do the Jenner et al. (2012) MORB glasses which show that these two elements are not affected by degassing at the higher S contents (Fig. 7). Therefore, only the higher S content basalts should be used to estimate the Cd and Bi content of the lunar mantle. In and Sn, on the other hand, show no evidence for degassing with lunar Sn and In in the low S glasses contiguous with the high S glasses. This suggests that lunar basalt In and Sn contents reflect the undegassed mantle melts and have not been lowered by degassing.

Using the trends defined by Cd-Yb, Bi-Yb, In-Yb, and Sn-Sm in lunar basalts, it is possible to estimate the mantle concentrations of these four elements in the lunar mantle (see the Processes Responsible for Depletions section). Our results are plotted in Fig. 1, and are 0.3, 0.02, 1, and 6 ppb, respectively. Our estimates for the lunar mantle are in good agreement with those made by Taylor and Wieczorek (2014). However, comparison to those of Hauri et al. (2015) shows significant disagreement for Cd, Bi, and Sn. The Hauri et al. (2015) lunar mantle estimates for these three elements are a factor of 10–100 times higher than ours (Fig. 7), due to the assumptions made by these authors. Their mantle concentrations are based on a reconstructed undegassed melt composition that is hinged on S degassing coupled with analyses of a volatile element-bearing surface coating. The Hauri et al. (2015) estimates are based on the assumption that the lunar basalt suites have degassed nearly 100% of their volatile elements such as Bi, Cd, and Zn. It is our contention, however, that if such high degassing rates were real, Cd/Dy and Bi/Dy should be strongly negatively correlated with sulfur, and such trends are not observed (Fig. 7). Instead they suggest only moderate degrees of degassing, similar to the terrestrial glass suites from Hawai'i (Norman et al. 2004). In addition, moderately volatile elements, like Ge and Ga, should be more depleted if there were extensive degassing, but they are not.

#### Mars Mantle

Degassing has also been proposed for many Martian basalts, and Martian basalt could thus also represent degassed magmas. Cd/Dy and Bi/Dy versus S trends (again, suggested by Norman et al. [2004] as an indicator of extent of degassing) shows that Martian basalts with the lowest S contents may have degassed Cd and Bi by a factor of five from those at intermediate S contents. The intermediate to high S content glasses show a slight increase in Cd/Dy and Bi/Dy with decreasing S content as do the Jenner et al. (2012)

MORB glasses which show that these two elements are not affected by degassing at the higher S contents. Therefore, as with the lunar basalt suites, only the higher S content basalts should be used to estimate the Cd and Bi content of the Martian mantle. In and Sn, on the other hand, show no evidence for degassing with Martian Sn and In in the low S glasses contiguous with the high S glasses. This suggests that Martian basalt In and Sn contents reflect the undegassed mantle melts and have not been lowered by degassing.

Using the trends defined by Cd-Yb, Bi-Yb, In-Yb, and Sn-Sm, then, it is possible to estimate the mantle concentrations of these four elements in the Martian mantle. Our results are plotted in Fig. 1, and are 6, 0.3, 9, and 60 ppb, respectively. These concentrations compare well with the estimates for Mars by Taylor (2013) and Yang et al. (2015) (Table 6; Fig. 1).

#### Volatility Correction for Bulk Composition Estimates

Using these new mantle estimates combined with previous work on terrestrial (Palme and O'Neill 2014), lunar (Righter 2002), and Martian bulk composition (Lodders and Fegley 1997), we can estimate the  $D(i)$  metal/silicate required if the VSE contents are due to core formation alone. However, because volatility affects some of the elements, we first have to correct the bulk compositions using the volatile lithophile elements as a guide. For example, for Earth, Bi, Cd, In, and Sn are all at low condensation temperatures (<800 K) where the lithophile volatile elements are also depleted, and this volatility must be accounted for (Fig. 8). Accordingly, Bi, Cd, In, and Sn are lower in the bulk Earth composition by a factor of 10, 10, 4, and 10, respectively. We use the volatility correction of Righter et al. (2017a, 2017b) for In, which utilizes a 50% condensation temperature of 800 K instead of 536 K. Similar corrections can be made for Mars using Lodders and Fegley (1997) bulk Mars compositions, and volatility corrections of 4, 5, 1.5, and 2, respectively (Fig. 8B). The bulk Moon is taken as terrestrial upper mantle and assuming a 4–5× volatile element depletion of lunar material relative to Earth as shown by Taylor and Wieczorek (2014) (Fig. 8C). All of these mantle, bulk, and volatility corrections are summarized in Table 6.

#### Metal-Silicate Partitioning

##### Regressions

Indium and Sn have been studied previously in some detail (Table S1, section 4). The effects of temperature and pressure were examined across a wide  $PT$  range and the effect of S on  $D(\text{In})$  and  $D(\text{Sn})$  metal/silicate has been determined (Righter and Drake 2000; Mann et al. 2009;

Ballhaus et al. 2013; Wang et al. 2016; Righter et al. 2017a,b). The effect of Si has only been measured for In, and Si clearly causes a reduction in  $D(\text{In})$ . Cadmium has been studied at the reconnaissance level by Ballhaus et al. (2013) and Wang et al. (2016). There are no previous partitioning data for Bi that we could find—our results seem to be the first reported. All partitioning data have been combined and regression was performed to create predictive expressions for  $D(i)$  metal/silicate according to this equation which has been derived elsewhere (Righter et al. 2017a, 2017b; Table 7; Table S1, section 5).

$$\ln D(i) = a \ln f\text{O}_2 + b/T + cP/T + \ln \gamma_i + g[nbo/T] + h \quad (1)$$

The  $a$  terms ( $\ln f\text{O}_2$ ) in Table 7 are consistent with  $\text{Sn}^{2+}$ ,  $\text{In}^{3+}$ , and  $\text{Cd}^{2+}$ , as expected and demonstrated previously. Temperature causes an overall decrease in  $D(i)$  metal/silicate. Pressure terms are positive, and thus might be expected to cause increase in  $D(i)$  metal/silicate, but pressure is coupled with the absolute  $\ln f\text{O}_2$  such that increase in pressure is associated with increase in  $f\text{O}_2$  which causes (especially for high valence elements) a decrease in  $D(i)$ . The activity coefficient of each element,  $\ln \gamma_i$ , is calculated using the  $\epsilon$  interaction parameter model of Righter et al. (2017a, 2017b) with additional  $\epsilon$  interaction parameters and  $\gamma_0$  values for Cd and Sn added (Table S1, section 2). Use of a different activity model for these elements yields similar results, indicating the reliability of the activity calculations (Table S1, section 3). Carbon and silicon dissolved in Fe metallic liquid both cause a decrease in  $D$  for all four of these elements. On the other hand, S causes all to increase, consistent with the chalcophile behavior traditionally assumed for these elements; Bi and Cd are the most chalcophile, whereas Sn and In are weakly chalcophile.

#### Application to Core Formation

Now having estimates for bulk composition, mantle composition, and partition coefficients relevant to core formation, we can interpret the cause of Bi, Cd, Sn, and In contents of mantles. The partitioning expressions can be combined with simple equilibrium differentiation calculations to estimate the mantle concentrations after core formation (from Righter et al. 2016):

$$C_{\text{LS}}^i = \frac{C_{\text{bulk}}^i}{x[p + (1-p)D_{\text{SS/LS}}^i] + (1-x)[D_{\text{LM/LS}}^i]} \quad (2)$$

where  $x$  is the fraction of silicate,  $p$  is the fraction of molten silicate,  $C_{\text{bulk}}^i$  is the bulk concentration of siderophile element,  $C_{\text{LS}}^i$  is the concentration of

Table 6. Bulk, mantle, and volatility values for calculations.

	Starting comp.	Volatility	Bulk (ppb)	Mantle (ppb) this study	Mantle (ppb) literature	
Earth	CI				Palme and O'Neill (2014)	
Bi	110 (10)	10	11.0	3 (1)	3 (1)	
Cd	674 (47)	10	67.4	35 (7)	35 (7)	
In	77.8 (3.9)	4	19.5	19 (4)	19 (4)	
Sn	1630 (245)	10	163	140 (15)	140 (15)	
Yb	0.169 (5)	–	0.169	0.477 (48)	0.477 (48)	
Dy	0.256 (7)	–	0.256	0.724 (72)	0.724 (72)	
Sm	0.154 (5)	–	0.154	0.435 (44)	0.435 (44)	
Mars	Lodders and Fegley (1997)				Taylor (2013)	
Bi	25	4	6.25	0.3 (0.15/1.1)	0.6	
Cd	80	5	16	10 (3/15)	9.6	
In	16	1.5	10.6	9 (4/20)	6.9	
Sn	915	2	457.5	60 (15/100)	38.5	
Yb	0.22	–	0.22	0.308	0.308	
Dy	0.36	–	0.36	0.45	0.45	
Sm	0.20	–	0.20	0.274	0.274	
Moon	Earth PUM				Hauri et al. (2015)/Taylor and Wieczorek (2014)	Hauri 74220
Bi	3 (1)	4	0.75	0.02 (0.01/0.08)	0.22/0.02	
Cd	35 (7)	4	5	0.3 (0.15/0.9)	11.7/0.31	149
In	19 (4)	4	4.75	1 (0.7/2.5)	1.6/–	15
Sn	140 (15)	4	35	6 (2/10)	39/–	
Yb	0.477 (48)	–	0.477	0.463/0.477	0.463/0.477	5
Dy	0.724 (72)	–	0.724	0.705/0.724	0.705/0.724	10
Sm	0.435 (44)	–	0.435	0.425/0.435	0.425/0.435	7

siderophile element in the liquid silicate,  $D_{SS/LS}^i$  is the partition coefficient between solid silicate and liquid silicate ( $<0.1$  for all elements here), and  $D_{LM/LS}^i$  ( $= D(i)$  from Equation 1 here) is the partition coefficient between LM and liquid silicate using the regression coefficients in Table 7. For Earth calculations,  $x = 0.68$  and  $p = 0.6$ ; for Moon,  $x = 0.985$  and  $p = 1.0$ ; and for Mars,  $x = 0.78$  and  $p = 0.6$  (from Righter 2011; Sharp et al. 2015; Yang et al. 2015; respectively).

### Earth

For Earth, melting during accretion to depths corresponding to  $PT$  conditions of 40–60 GPa and 3500–4000 K causes lowering of  $D(i)$  metal/silicate for a wide range of elements such as Ni, Co, Mo, W, As, Sb, and Ge (Righter 2011; Siebert et al. 2011, 2013; Righter et al. 2016). Following the approach of Righter et al. (2017a, 2017b), the S, C, and Si content of the core FeNi metal can be calculated as accretion proceeds with increasing pressure and temperature and  $fO_2$  changing from reduced to oxidized (IW–4 to IW–2). The core composition (Fe, Ni, S, C, and Si) can then be used to calculate the activity coefficient and thus  $D(\text{metal/silicate})$  for the VSE using Equation 1. Coupling the calculated values of  $D(\text{Cd})$ ,  $D(\text{Sn})$ , and  $D(\text{In})$  metal/

silicate with Equation 2, and assuming metal-silicate equilibration occurs rapidly during rainfall through the mantle (Kendall and Melosh 2016) allow calculation of the mantle concentrations of Bi, Cd, In, and Sn. Note that these values are assuming and corrected for volatile element depletion. The calculated values of Cd, Sn, and In approach those measured in the Earth's mantle at higher  $PT$  conditions (Fig. 9), and suggest that the concentrations of these three volatile elements could have been established in the mantle by early metal-silicate equilibrium. There is not enough  $D(\text{Bi})$  metal/silicate data to calculate  $D(\text{Bi})$  metal/silicate at these high  $PT$  conditions, but our results show that  $D(\text{Bi})$  metal/silicate is lowered at high temperatures to values  $\sim 5.0$  which would be needed if Bi content of mantle was due only to metal-silicate equilibrium (Fig. 4).

*Hadean Matte?*: The origin of sulfur and other chalcophile elements in the Earth's mantle has been debated for some time. One hypothesis is the low S content of 250 ppm was established by segregation of a sulfide matte from the mantle into the core after the Hadean Earth had differentiated (Arculus and Delano 1981; O'Neill 1991). Accumulation and evaluation of high- $PT$  metal-silicate partitioning for S has led to the possibility that S content is due to equilibration of

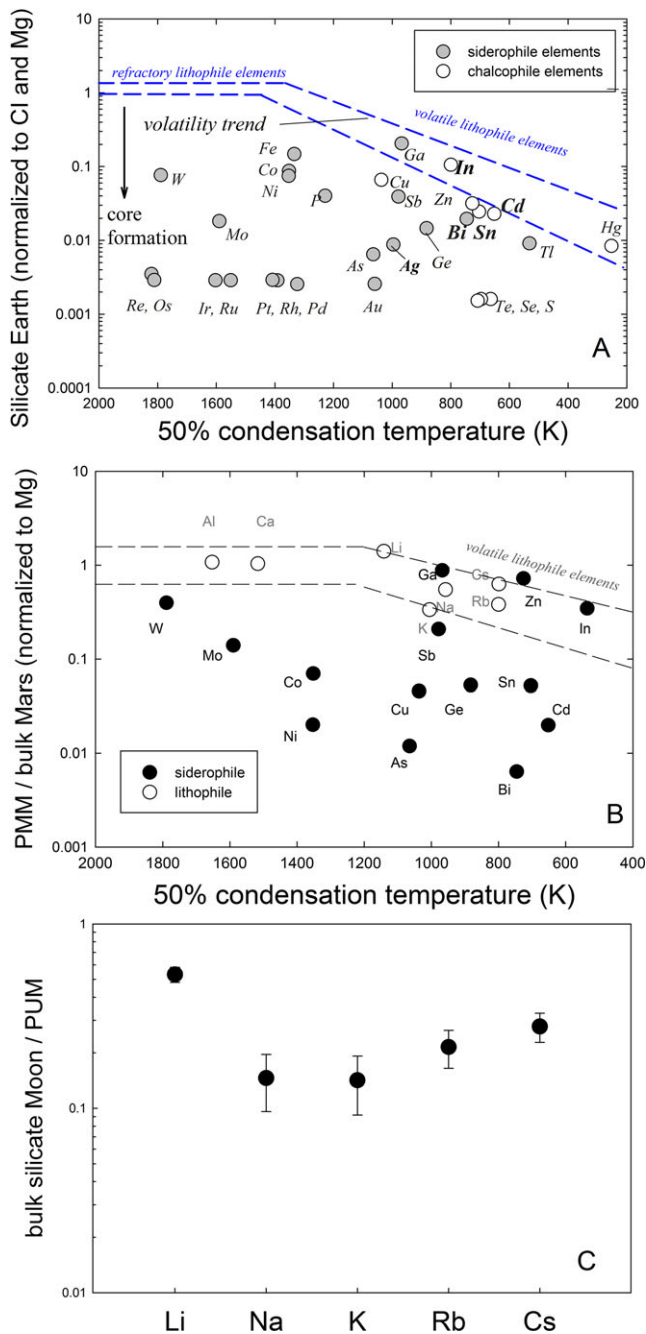


Fig. 8. A) Concentrations of siderophile elements in the terrestrial primitive upper mantle, relative to CI chondrites, plotted against 50% condensation temperature for the metal (modified from Righter et al. 2017a, 2017b). Depletions of volatile siderophile elements are due in part to volatility, as shown by the region between dashed lines. In, Bi, Sn, and Cd plot within or below the volatility trend indicating that a further depletion is likely due to core formation. Volatility corrections for Bi, Cd, In, and Sn are 10, 10, 4, and 10, respectively, based on this figure and the discussions in the text. B) Estimates for the primitive Martian mantle for siderophile compared to lithophile elements. Note that Zn and In are roughly aligned with the trend of lithophile volatile elements Li, Na, Cs, and Rb, suggesting no significant partitioning into the core, while Bi, Cd, and Sn are all much lower than this lithophile volatile element trend. Bulk Mars data from Lodders and Fegley (1997), and mantle estimates from Yang et al. (2015) and Taylor (2013). C) Depletion of Li, Na, K, Rb, and Cs in the lunar mantle relative to the terrestrial mantle illustrating the overall depletion of the Moon in volatile elements. Data from Taylor and Wieczorek (2014), Warren (2005), and Taylor (1982), normalized to terrestrial PUM values of Palme and O'Neill (2014).

sulfide would reduce the Bi content of the mantle by a factor of 2, and Cd, Sn, and In even less. So, even though these elements are all chalcophile, their concentrations will be mostly insensitive to sulfide fractionation. Bi, Cu, and Ni all with  $D(\text{sulfide/silicate})$  near 1000–2000 will be affected most and should be the focus of future modeling efforts, along with the HSE. Additionally, dissolved Si in core-forming liquids has a stronger and opposite effect than dissolved S for many chalcophile elements (In, Sb, and As) and must be carefully quantified together with the role of sulfide.

Wang et al. (2016) stated that In is always more siderophile than Cd and Zn, and thus that the depletions of In, Cd, and Zn must have an explanation other than core formation. However, there are two aspects of these elements to bear in mind. First, the Wang et al. (2016) interpretation hinges on the value of the In 50% condensation temperature. A metal-based value is near 536 K (e.g., Palme and O'Neill 2014), while a sulfide-based value is near 800 K (Righter et al. 2017a). The latter would make the  $D(\text{In})$  and  $D(\text{Zn})$  metal/silicate required for equilibrium to be about the same and  $<1$ . Second,  $D(\text{In})$  metal/silicate can actually be lower than  $D(\text{Cd})$  for metallic Fe liquids with high S content, which is observed here and in the studies of Wood et al. (2014) and Kiseeva and Wood (2013). On the other hand, dissolved Si reduces  $D(\text{In})$  greater than for  $D(\text{Cd})$  and  $D(\text{Zn})$  metal/silicate (Righter et al. 2017a, 2017b). Thus, the combination of a S- and Si-bearing metallic core will drive  $D(\text{In})$  lower and  $D(\text{Cd})$  higher. Resolution of the degree of siderophilicity of  $D(\text{In})$ ,  $D(\text{Zn})$ , and  $D(\text{Cd})$  metal/silicate for terrestrial core

metal and silicate in a deep magma ocean (Boujibar et al. 2014), but debate continues (Ballhaus et al. 2017). Some recent constraints on a sulfide matte were provided by the highly siderophile elements (with  $D(\text{sulfide/silicate}) \sim 10,000$ ), and suggest that segregation of 1–2% of sulfide can lower HSE concentrations in primitive mantle to values observed today. Because all elements studied here are considered chalcophile (Wood et al. 2014; this study), they might also be useful in evaluating these and other models. Removal of 1–2%

Table 7. Regression coefficients for Sn, Cd, In, and Zn (for use in Equation 1 in table note).

Element	a	b	c	g	h	$r^2$	$2\sigma$	$N$	References
Sn	-0.75 (6)	-47300 (4000)	850 (200)	+0.27 (17)	+11.9 (2.5)	0.86	1.20	93	1,2,5,6,7,8
In	-1.07 (21)	-75900 (15500)	1336 (290)	+0.09 (4)	+20.7 (5.0)	0.61	0.90	60	1,2,3,9,10
Cd	-0.69 (9)	-45500 (6700)	848 (120)	+0.09 (8)	+9.8 (2.2)	0.88	0.73	41	1,2,3,4
Zn	-0.76 (6)	-48650 (4500)	890 (90)	+0.16 (9)	+6.78 (1.4)	0.81	0.61	95	Sources in 11

1—This study; 2—Ballhaus et al. (2013); 3—Wang et al. (2016); 4—Wood et al. (2014); 5—Capobianco et al. (1999); 6—Righter and Drake (2000); 7—Righter et al. (2008a, 2008b); 8—Righter et al. (2010); 9—Mann et al. (2009); 10—Righter et al. (2017a, 2017b); 11—Yang et al. (2015).

Equation (1):  $\ln D(i) = a \ln fO_2 + b/T + cP/T + \ln \gamma_i + g[nbo/t] + h$ .

formation conditions depends on how much S and Si are in the core—a topic of active debate (Labidi et al. 2013; Badro et al. 2015; Savage et al. 2015), and will benefit from additional studies.

### Mars

For Mars, previous work on core formation has shown that the siderophile element abundances may have been set by metal-silicate equilibrium in an intermediate depth magma ocean near 14 GPa and 2400 K (Righter and Chabot 2011; Rai and Van Westrenen 2013; Yang et al. 2015). As with the Earth, one can calculate the S, C, and Si content of the metallic FeNi core during the accretion of Mars, and thus calculate the activity coefficient for each element. For Mars, the core composition is more S-rich than Earth, and does not contain significant Si, due to the lower pressures and higher  $fO_2$  of the Martian interior. Combining Equations 1 and 2 then one calculates mantle concentrations of Cd, Sn, and In that approach the Mars mantle values estimated by Taylor (2013) (Fig. 10). There is not enough  $D(\text{Bi})$  metal/silicate data to calculate  $D(\text{Bi})$  metal/silicate at these  $PT$  conditions for Mars, but our data show that  $D(\text{Bi})$  is expected to be  $\sim 100$  at 2000 °C and for a 10% S core expected for Mars (Fig. 4). This is not dissimilar to  $D(\text{Bi})$  metal/silicate = 91 implied by the mantle and bulk composition estimates for Mars (Table 6). Thus, the concentrations of these four VSE could have been established in the mantle by early metal-silicate equilibrium for Mars, too.

### Moon

For Moon, there is some uncertainty as discussed in the Moon Mantle section above, due to interpretation of depletions. If core formation took place at 2100 °C, 4 GPa, at IW-2 for lunar mantle composition and S- and C-poor core, we can calculate  $D(\text{In})$ ,  $D(\text{Cd})$ ,  $D(\text{Sn})$  metal/silicate, and estimate  $D(\text{Bi})$  metal/silicate based on our results here. The resulting mantle concentrations of Cd, Sn, In, and Bi are generally higher than those derived from Apollo samples

(Figs. 11A and 11B). The Hauri et al. (2015) lunar mantle estimates have the same overall shape of concentrations, but Cd, In, Zn, and especially Bi are all lower, while Sn is higher than the calculated postcore formation mantle (Fig. 11A). The lunar mantle estimates derived here and by Taylor and Wieczorek (2014) also have the same overall shape of concentrations, but all five of these highly volatile elements are lower than expected from core formation (Fig. 11B). In fact the depletions can only be matched using  $D$  metal/silicate values that are orders of magnitude higher than any that have been measured in the laboratory. For example, compare  $D(\text{Bi})$  metal/silicate = 10,000,  $D(\text{Sn})$  metal/silicate = 412,  $D(\text{In})$  metal/silicate = 200, and  $D(\text{Cd})$  metal/silicate = 3700, to those values measured experimentally in Fig. 4. In this latter case, it is clear that an additional explanation or mechanism is required to explain the rest of the depletion—core formation only explains part of the mantle depletion. In both cases, the calculated values mimic the depletions observed, but offset to higher concentrations. This suggests the depletions have a link to the degree of siderophility.

What is the explanation for the additional depletions? We will consider two possibilities here—that the elemental trends examined for lunar samples lead to erroneous mantle concentrations, or that the estimates of the highly volatile element concentrations in the bulk Moon are erroneously high.

Maybe the use of the basalt trends are leading to an incorrect mantle value due to larger amounts of magmatic degassing than indicated by the trace element variations. Hauri et al. (2015) suggested that degassing rates for many volatile elements (Zn, In, and S) are very high—some even 98–100%. However, these high degassing rates are not supported by a number of different views. First, S elemental and isotopic analyses indicate degassing is limited to 50% at most, and usually less (Wing and Farquhar 2015). Second, evidence from the lunar S-Cd, S-Bi (Fig. 7 and also see McCubbin et al. 2015), and S-In indicates that lunar degassing is limited and not as severe as the Hauri et al.



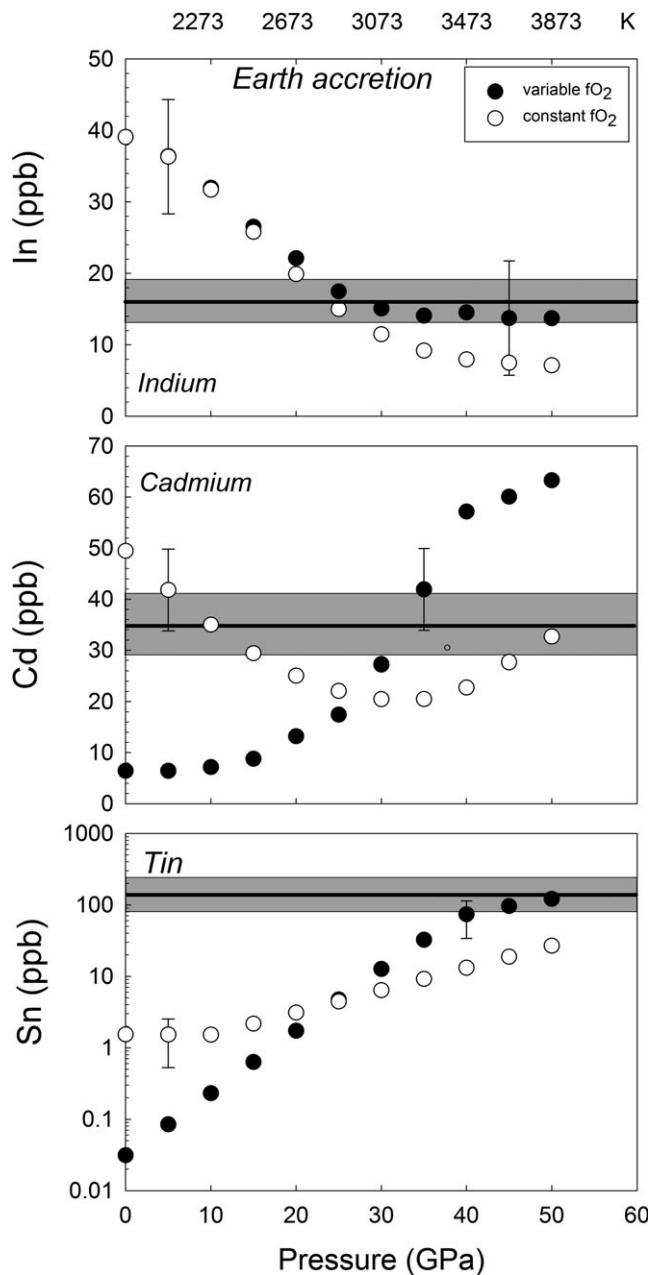


Fig. 9. Evolution of Earth's mantle In, Cd, and Sn as accretion proceeds for two different scenarios: accretion with  $f_{O_2}$  nearly constant (open circles), and  $f_{O_2}$  increasing from IW-4 to IW-2 (closed circles);  $PT$  curve for calculations is along peridotite liquidus of Fiquet et al. (2010). Horizontal gray bands and solid lines represent terrestrial primitive upper mantle values (and associated uncertainty) for each element, from Table 6. Error bars on the calculated values include  $2\sigma$  error from the partitioning regressions (Table 7), as well as uncertainty from the volatility correction for the bulk Earth concentrations; one typical error bar is shown to maximize clarity in presentation. Changing Fe metallic liquid composition has a large effect on the activity coefficients of Cd, In, and Sn in Fe metallic liquids. The final core composition for this second model is 10.2% Si, 2% S, and 1.1% C (or  $X_{Si} = 0.18$ ,  $X_S = 0.03$ , and  $X_C = 0.04$ ).

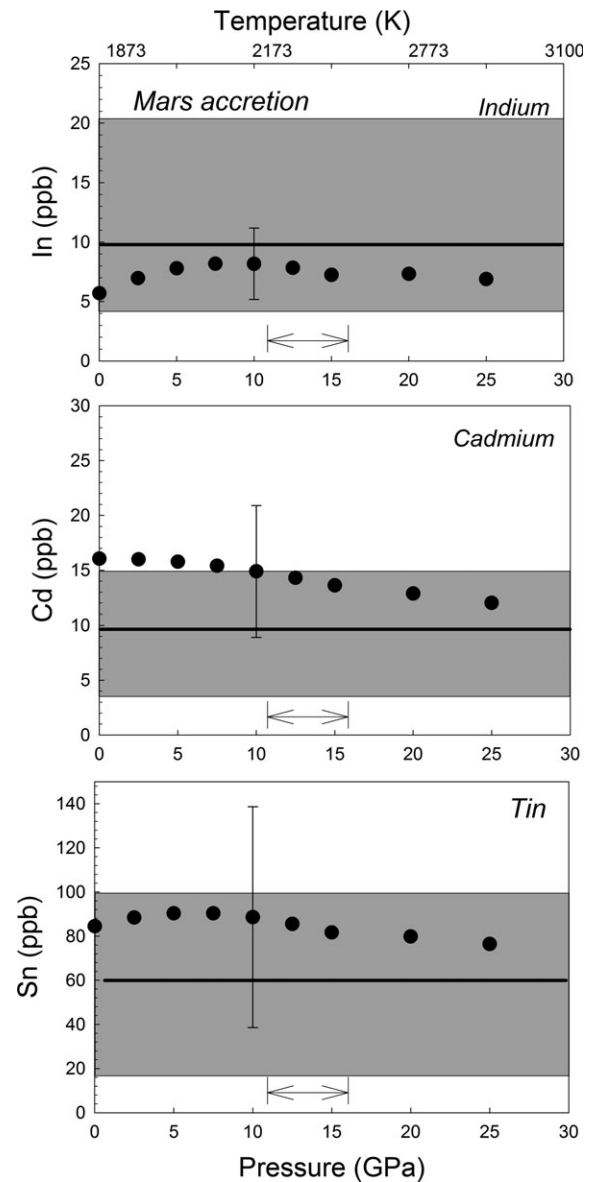


Fig. 10. Comparison of In, Sn, and Cd abundances in the Martian mantle (horizontal gray band and solid line) to core formation model results (solid circles) plotted as a function of pressure (GPa) and temperature (K). Using the regressions derived for In, Sn, and Cd from Table 7, we can examine the evolution of the composition of Mars' mantle during accretion to compare to the Martian mantle estimates. Error bars on the calculated values include  $2\sigma$  error from the partitioning regressions (Table 7), as well as uncertainty from the volatility correction for the bulk Mars concentrations; one typical error bar is shown to maximize clarity in presentation. Calculations have been carried out along the  $PT$  conditions of the liquidus for the Martian magma ocean (from Yang et al. 2015), using the bulk mantle composition of Longhi et al. (1992), metallic liquid with  $X_S = 0.05$  and  $X_C = 0.12$ , oxygen fugacity of  $\Delta IW = -1.5$ , and assuming equilibration during the accretion steps. Also shown along the bottom of each panel is the range of pressures at which other siderophile elements (Ni, Co, Mo, W, P, Mn, Cr, V, and HSE) can be explained by equilibrium partitioning as well (Righter and Chabot 2011; Righter et al. 2015; Yang et al. 2015).

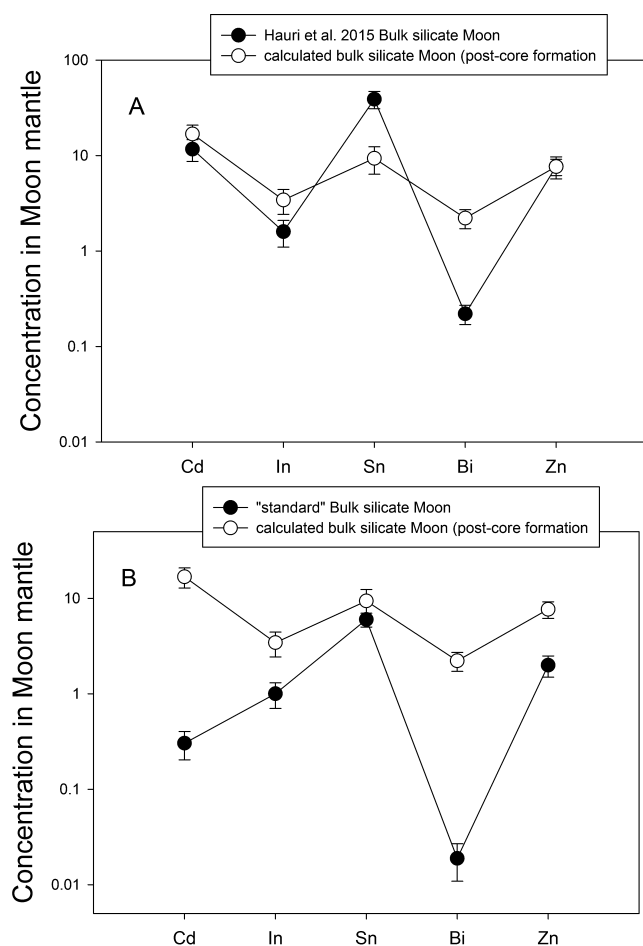


Fig. 11. A) Concentrations of volatile elements Cd, In, Sn, Bi, and Zn in the bulk silicate Moon from Hauri et al. (2015) (black circles), compared to bulk silicate Moon calculated after segregation of a small lunar core using partitioning data (open circles). B) Concentrations of volatile elements Cd, In, Sn, Bi, and Zn in the bulk silicate Moon from Taylor and Wicczorek (2014) compared to bulk silicate Moon calculated after segregation of a small lunar core using partitioning data (open circles). For the calculated values, the bulk Moon has primitive terrestrial upper mantle composition, and a 1.5 mass% core. The calculated postcore formation mantle concentrations are generally higher than those derived by Taylor and Wicczorek (2014), whereas they compare well with Cd, In, and Zn bulk silicate Moon derived by Hauri et al. (2015), but Bi is lower and Sn is higher. See text for additional discussion. Error bars on the calculated values include  $2\sigma$  error from the partitioning regressions (Table 7), as well as uncertainty from the volatility correction for the bulk Moon concentrations.

(2015) estimates, which are based on one glass bead analysis. Third, there is no apparent correlation between diffusion and mobility measured experimentally (MacKenzie and Canil 2008; Johnson and Canil 2011) and the degree of depletion. For example, at 1200 °C, Cd and As have higher diffusion coefficients than Bi or Pb

(e.g., MacKenzie and Canil 2008), yet Bi has a larger depletion. If magmatic degassing were a widespread and common process, suites of basalts should show abundant evidence for degassing, but they do not.

Maybe the bulk Moon VSE estimates are incorrect? The BSE composition is well known and the assumption of similarity of the composition of the Moon to Earth is supported by a number of important observations including refractory (Ca, Ti, Mg, and Si) and oxygen isotopes (Simon and DePaolo 2010; Zhang et al. 2012; Dauphas et al. 2014; Herwartz et al. 2014; Young et al. 2016). The consistent finding that the Moon is depleted in moderately volatile elements relative to the Earth by a factor of 4–5 seems robust and is supported by a wide range of lithophile elements, Li, Na, K, Rb, and Cs (Fig. 8C), and even some moderately VSE such as Ge and Sb (Richter et al. 2009, 2011). But there is no reason a priori why the Moon should also be depleted to this same level for the highly volatile elements. It seems reasonable and likely that the Moon is depleted in highly volatile elements to a greater extent than the moderately volatile elements and that this could have occurred during the giant impact event. Future work on the origin of lunar volatiles should perhaps focus on distinguishing these classes of elements rather than focusing on one or the other.

In summary, explanations for the lunar VSE include two possibilities, i.e., (1) accepting the Hauri et al. (2015) bulk silicate Moon concentrations, which leads to the conclusion that moderately and some of the highly volatile elements are consistent with core formation plus volatility inherited from Earth and giant impact (Sb, Ge, Ga, Zn, In, and Cd), but Sn is too high and Bi is too low; or (2) accepting the bulk silicate Moon concentrations derived here and by Taylor and Wicczorek (2014), which leads to the possibility that the moderately (Sb, Ge, and Ga), but none of the highly volatile elements are consistent with core formation plus volatility inherited from Earth and the giant impact. Cd, In, Zn, Sn, and Bi would all require an additional depletion that may be caused by and occurred during the giant impact. Regardless of which hypothesis is correct, relative patterns reflect a core formation event because the severity of the depletion is correlated with the magnitude of the metal/silicate partition coefficient.

## CONCLUSIONS

High temperatures during metal segregation can reduce the magnitude of  $D(\text{Bi, Sn, and In})$  metal/silicate and  $\ln K_D$  (Fe-M exchange coefficient).  $D(\text{Cd})$  and  $\ln K_D$  (Fe-Cd), on the other hand, slightly increase across the same temperature range. The effect of pressure was studied in the range relevant to the Moon and found to

be minimal. The effect of S and C has also been investigated with S exhibiting an overall increase in  $D$  (Bi) and  $D$ (Cd) metal/silicate, and only a weak increase for  $D$ (Sn) and  $D$ (In) metal/silicate. Carbon appears to decrease  $D(i)$  metal/silicate for all four elements. Sulfur and C are only two representatives of what may be several other light elements in the core and thus comprise a partial understanding of the effect of metal composition. The role of Si and O on metal/silicate partitioning of all four elements will be important to quantify in future studies. Combination of our data with data from the literature shows the effects of  $P$ ,  $T$ ,  $fO_2$ , and composition, and allows application to interpretation of depletions of Bi, Cd, In, and Sn, in mantles of the Earth, Moon, and Mars. Earth and Mars mantle contents can be explained by metal-silicate equilibrium, whereas lunar mantle contents are more severely depleted than expected from core formation alone. The additional depletions may have been caused by volatile loss during the giant impact, or magma ocean degassing.

*Acknowledgments*—This work was supported by RTOPs to K. Righter from the NASA Cosmochemistry and LASER programs. N. Marin was supported by an LPI Summer Internship. Discussions with F. McCubbin, A. Saal, and J. Taylor were beneficial to interpretations presented here. We acknowledge the helpful reviews of K. Mezger, an anonymous reviewer, and the associate editor K. Joy.

*Editorial Handling*—Dr. Katherine Joy

## REFERENCES

- Adam J. and Green T. 2006. Trace element partitioning between mica-and amphibole-bearing garnet lherzolite and hydrous basanitic melt: 1. Experimental results and the investigation of controls on partitioning behaviour. *Contributions to Mineralogy and Petrology* 152:1–17.
- Albarede F. 2009. Volatile accretion history of the terrestrial planets and dynamic implications. *Nature* 461:1227–1233.
- Arculus R. J. and Delano J. W. 1981. Siderophile element abundances in the upper mantle: Evidence for a sulfide signature and equilibrium with the core. *Geochimica et Cosmochimica Acta* 45:1331–1343.
- Badro J., Brodholt J. P., Piet H., Siebert J., and Ryerson F. J. 2015. Core formation and core composition from coupled geochemical and geophysical constraints. *Proceedings of the National Academy of Sciences* 112:12,310–12,314.
- Ballhaus C., Laurenz V., Münker C., Fonseca R. O., Albarède F., Rohrbach A., and Weis U. 2013. The U/Pb ratio of the Earth's mantle—A signature of late volatile addition. *Earth and Planetary Science Letters* 362:237–245.
- Ballhaus C., Fonseca R. O., Münker C., Rohrbach A., Nagel T., Speelmanns I. M., and Heuser A. 2017. The great sulfur depletion of Earth's mantle is not a signature of mantle–core equilibration. *Contributions to Mineralogy and Petrology* 172:68–75.
- Barnes J. J., Tartese R., Anand M., McCubbin F. M., Neal C. R., and Franchi I. A. 2016. Early degassing of lunar urKREEP by crust-breaching impact(s). *Earth and Planetary Science Letters* 447:84–94.
- Basaltic Volcanism Study Project (BVSP). 1981. *Basaltic volcanism on the terrestrial planets*. Houston, Texas: Pergamon Press. 1282 pp.
- Boujibar A., Andrault D., Bouhifd M. A., Bolfan-Casanova N., Devidal J. L., and Trcera N. 2014. Metal-silicate partitioning of sulphur, new experimental and thermodynamic constraints on planetary accretion. *Earth and Planetary Science Letters* 391:42–54.
- Burghelle A., Dreibus G., Palme H., Rammensee W., Spettel B., Weckworth G., and Wänke H. 1984. Chemistry of shergottites and the shergotty parent body (SPB): Further evidence for the two component model of planet formation. *Proceedings, 14th Lunar and Planetary Science Conference*. pp. 80–81.
- Campbell A. J., Danielson L., Righter K., Seagle C. T., Wang Y., and Prakapenka V. B. 2009. High pressure effects on the iron–iron oxide and nickel–nickel oxide oxygen fugacity buffers. *Earth and Planetary Science Letters* 286:556–564.
- Capobianco C. J., Drake M. J., and de'Aro J. 1999. Siderophile geochemistry of Ga, Ge, and Sn: Cationic oxidation states in silicate melts and the effect of composition in iron–nickel alloys. *Geochimica et Cosmochimica Acta* 63:2667–2677.
- Dauphas N., Burkhardt C., Warren P. H., and Fang-Zhen T. 2014. Geochemical arguments for an Earth-like Moon-forming impactor. *Philosophical Transactions of the Royal Society of London A: Mathematical, Physical and Engineering Sciences* 372:20130244.
- Drake M. J., Newsom H. E., and Capobianco C. J. 1989. V, Cr, and Mn in the Earth, Moon, EPB, and SPB and the origin of the Moon: Experimental studies. *Geochimica et Cosmochimica Acta* 53:2101–2111.
- Fiquet G., Auzende A. L., Siebert J., Corgne A., Bureau H., Ozawa H., and Garbarino G. 2010. Melting of peridotite to 140 gigapascals. *Science* 329:1516–1518.
- Gee L. L. and Sack R. O. 1988. Experimental petrology of melilite nephelinites. *Journal of Petrology* 29:1233–1255.
- Hauri E. H., Saal A. E., Rutherford M. J., and Van Orman J. A. 2015. Water in the Moon's interior: Truth and consequences. *Earth and Planetary Science Letters* 409:252–264.
- Hertogen J., Janssens M. J., and Palme H. 1980. Trace elements in ocean ridge basalt glasses: Implications for fractionations during mantle evolution and petrogenesis. *Geochimica et Cosmochimica Acta* 44:2125–2143.
- Herwartz D., Pack A., Friedrichs B., and Bischoff A. 2014. Identification of the giant impactor Theia in lunar rocks. *Science* 344:1146–1150.
- Hohl S. V., Galer S. J. G., Gamper A., and Becker H. 2017. Cadmium isotope variations in Neoproterozoic carbonates—A tracer of biologic production? *Geochemical Perspective Letters* 3:32–44.
- Holzheid A., Palme H., and Chakraborty S. 1997. The activities of NiO, CoO and FeO in silicate melts. *Chemical Geology* 139:21–38.
- Horner T. J., Lee R. B., Henderson G. M., and Rickaby R. E. 2013. Nonspecific uptake and homeostasis drive the

- oceanic cadmium cycle. *Proceedings of the National Academy of Sciences* 110:2500–2505.
- Jenner F. E. and O'Neill H. S. C. 2012. Analysis of 60 elements in 616 ocean floor basaltic glasses. *Geochemistry, Geophysics, Geosystems* 13.
- Jenner F. E., Arculus R. J., Mavrogenes J. A., Dyriw N. J., Nebel O., and Hauri E. H. 2012. Chalcophile element systematics in volcanic glasses from the northwestern Lau Basin. *Geochemistry, Geophysics, Geosystems* 13.
- Jochum K. P., Hofmann A. W., and Seufert H. M. 1993. Tin in mantle-derived rocks: Constraints on Earth evolution. *Geochimica et Cosmochimica Acta* 57:3585–3595.
- Jochum K. P., Weis U., Schwager B., Stoll B., Wilson S. A., Haug G. H., Andrae M. O., and Enzweiler J. 2016. Reference values following ISO guidelines for frequently requested rock reference materials. *Geostandards and Geoanalytical Research* 40:333–350. <https://doi.org/10.1111/j.1751-908X.2015.00392.x>.
- Johnson A. and Canil D. 2011. The degassing behavior of Au, Tl, As, Pb, Re, Cd and Bi from silicate liquids: Experiments and applications. *Geochimica et Cosmochimica Acta* 75:1773–1784.
- Karner J. M., Sutton S. R., Papike J. J., Shearer C. K., Jones J. H., and Newville M. 2006. Application of a new vanadium valence oxybarometer to basaltic glasses from the Earth, Moon, and Mars. *American Mineralogist* 91:270–277.
- Kendall J. D. and Melosh H. J. 2016. Differentiated planetesimal impacts into a terrestrial magma ocean: Fate of the iron core. *Earth and Planetary Science Letters* 448:24–33.
- Kiseeva E. S. and Wood B. J. 2013. A simple model for chalcophile element partitioning between sulphide and silicate liquids with geochemical applications. *Earth and Planetary Science Letters* 383:68–81.
- Labidi J., Cartigny P., and Moreira M. 2013. Non-chondritic sulphur isotope composition of the terrestrial mantle. *Nature* 501:208–211.
- Laul J. C., Kays R. R., Ganapathy R., Anders E., and Morgan J. W. 1972. Chemical fractionation in meteorites—V. Volatile and siderophile elements in achondrites and ocean ridge basalts. *Geochimica et Cosmochimica Acta* 36:329–345.
- Lewis R. D., Lofgren G. E., Franzen H. F., and Windom K. E. 1993. The effect of Na vapor on the Na content of chondrules. *Meteoritics* 28:622–628.
- Li J. and Agee C. B. 1996. Geochemistry of mantle-core formation at high pressure. *Nature* 381:686–689.
- Li Y. and Audétat A. 2015. Effects of temperature, silicate melt composition, and oxygen fugacity on the partitioning of V, Mn, Co, Ni, Cu, Zn, As, Mo, Ag, Sn, Sb, W, Au, Pb, and Bi between sulfide phases and silicate melt. *Geochimica et Cosmochimica Acta* 162:25–45.
- Lodders K. 1998. A survey of shergottite, nakhlite and chassigny meteorites whole rock compositions. *Meteoritics & Planetary Science* 33:A183–A190.
- Lodders K. and Fegley B. 1997. An oxygen isotope model for the composition of Mars. *Icarus* 126:373–394.
- Longhi J., Knittle E., Holloway J. R., and Wänke H. 1992. The bulk composition, mineralogy and internal structure of Mars. In *Mars* edited by Kieffer H. H. Tucson, Arizona: University of Arizona Press. 184–208.
- MacKenzie J. M. and Canil D. 2008. Volatile heavy metal mobility in silicate liquids: Implications for volcanic degassing and eruption prediction. *Earth and Planetary Science Letters* 269:488–496.
- Mann U., Frost D. J., and Rubie D. C. 2009. Evidence for high-pressure core-mantle differentiation from the metal-silicate partitioning of lithophile and weakly-siderophile elements. *Geochimica et Cosmochimica Acta* 73:7360–7386.
- McCubbin F. M., Kaaden K. E. V., Tartèse R., Klima R. L., Liu Y., Mortimer J., Barnes J. J., Shearer C. K., Treiman A. H., Lawrence D. J., and Elardo S. M. 2015. Magmatic volatiles (H, C, N, F, S, Cl) in the lunar mantle, crust, and regolith: Abundances, distributions, processes, and reservoirs. *American Mineralogist* 100:1668–1707.
- Meyer C. Jr., McKay D. S., Anderson D. H., and Butler P. Jr. 1975. The source of sublimates on the Apollo 15 green and Apollo 17 orange glass samples. *Proceedings, 6th Lunar Science Conference*. pp. 1673–1699.
- Newsom H. E. 1995. Composition of the solar system, planets, meteorites, and major terrestrial reservoirs. *Global Earth Physics* 1:159–189.
- Norman M. D., Garcia M. O., and Bennett V. C. 2004. Rhenium and chalcophile elements in basaltic glasses from Ko'olau and Moloka'i volcanoes: Magmatic outgassing and composition of the Hawaiian plume. *Geochimica et Cosmochimica Acta* 68:3761–3777.
- Norris C. A. and Wood B. J. 2017. Earth's volatile contents established by melting and vaporization. *Nature* 549:507–510.
- O'Neill H. S. C. 1991. The origin of the Moon and the early history of the Earth—A chemical model. Part 2: The Earth. *Geochimica et Cosmochimica Acta* 55:1159–1172.
- Palme H. and O'Neill H. S. C. 2014. Cosmochemical estimates of mantle composition. In *Planets, asteroids, comets, and the solar system*, edited by Davis A. M. Treatise on Geochemistry, vol. 2, 2nd ed. Elsevier, New York, pp. 1–39.
- Paniello R. C., Day J. M., and Moynier F. 2012. Zinc isotopic evidence for the origin of the Moon. *Nature* 490:376–380.
- Rai N. and Van Westrenen W. 2013. Core-mantle differentiation in Mars. *Journal of Geophysical Research: Planets* 118:1195–1203.
- Redfern S. A. T., Artioli G., Rinaldi R., Henderson C. M. B., Knight K. S., and Wood B. J. 2000. Octahedral cation ordering in olivine at high temperature. II: An in situ neutron powder diffraction study on synthetic MgFeSiO<sub>4</sub> (Fa<sub>50</sub>). *Physics and Chemistry of Minerals* 27:630–637.
- Righter K. 2002. Does the Moon have a metallic core? Constraints from giant impact modelling and siderophile elements. *Icarus* 158:1–13.
- Righter K. 2011. Prediction of metal-silicate partition coefficients for siderophile elements: An update and assessment of PT conditions for metal-silicate equilibrium during accretion of the Earth. *Earth and Planetary Science Letters* 304:158–167.
- Righter K. 2015. Modelling siderophile elements during core formation and accretion, and the role of the deep mantle and volatiles. *American Mineralogist* 100:1098–1109.
- Righter K. and Chabot N. L. 2011. Moderately and slightly siderophile element constraints on the depth and extent of melting in early Mars. *Meteoritics & Planetary Science* 46:157–176.
- Righter K. and Drake M. J. 1997. Metal-silicate equilibrium in a homogeneously accreting Earth: New results for Re. *Earth and Planetary Science Letters* 146:541–553.
- Righter K. and Drake M. J. 2000. Metal/silicate equilibrium in the early Earth—New constraints from the volatile moderately siderophile elements Ga, Cu, P, and Sn. *Geochimica et Cosmochimica Acta* 64:3581–3597.

- Righter K., Chesley J. T., Caiazza C. M., Gibson E. K., and Ruiz J. 2008a. Re and Os concentrations in arc basalts: The roles of volatility and source region  $fO_2$  variations. *Geochimica et Cosmochimica Acta* 72:926–947.
- Righter K., Humayun M., and Danielson L. 2008b. Partitioning of palladium at high pressures and temperatures during core formation. *Nature Geoscience* 1:321–323.
- Righter K., Humayun M., Campbell A. J., Danielson L., Hill D., and Drake M. J. 2009. Experimental studies of metal–silicate partitioning of Sb: Implications for the terrestrial and lunar mantles. *Geochimica et Cosmochimica Acta* 73:1487–1504.
- Righter K., Pando K. M., Danielson L., and Lee C. T. 2010. Partitioning of Mo, P and other siderophile elements (Cu, Ga, Sn, Ni, Co, Cr, Mn, V, and W) between metal and silicate melt as a function of temperature and silicate melt composition. *Earth and Planetary Science Letters* 291:1–9.
- Righter K., King C., Danielson L., Pando K., and Lee C. T. 2011. Experimental determination of the metal/silicate partition coefficient of Germanium: Implications for core and mantle differentiation. *Earth and Planetary Science Letters* 304:379–388.
- Righter K., Danielson L. R., Pando K. M., Williams J., Humayun M., Hervig R. L., and Sharp T. G. 2015. Highly siderophile element (HSE) abundances in the mantle of Mars are due to core formation at high pressure and temperature. *Meteoritics & Planetary Science* 50:604–631.
- Righter K., Danielson L. R., Pando K. M., Shofner G. A., Sutton S. R., Newville M., and Lee C. T. 2016. Valence and metal/silicate partitioning of Mo: Implications for conditions of Earth accretion and core formation. *Earth and Planetary Science Letters* 437:89–100.
- Righter K., Nickodem K., Pando K., Danielson L. R., Boujibar A., Righter M., and Lapen T. J. 2017a. Distribution of Sb, As, Ge, and In between metal and silicate during accretion and core formation in the Earth. *Geochimica et Cosmochimica Acta* 198:1–16.
- Righter K., Pando K., and Ross D. K. 2017b. Effect of silicon on activity coefficients of P, Bi, Cd, Sn, and Ag in liquid Fe–Si, and implications for differentiation and core formation. 80th Annual Meeting of the Meteoritical Society. LPI Contribution 1987. Houston, Texas: Lunar and Planetary Institute.
- Rubin K. 1997. Degassing of metals and metalloids from erupting seamount and mid-ocean ridge volcanoes: Observations and predictions. *Geochimica et Cosmochimica Acta* 61:3525–3542.
- Savage P. S., Moynier F., Chen H., Shofner G., Siebert J., Badro J., and Puchtel I. S. 2015. Copper isotope evidence for large-scale sulphide fractionation during Earth's differentiation. *Geochemical Perspectives Letters* 1:53–64.
- Schediwiy S., Rosman K. J. R., and De Laeter J. R. 2006. Isotope fractionation of cadmium in lunar material. *Earth and Planetary Science Letters* 243:326–335.
- Sharp M. G., Righter K., and Walker R. J. 2015. Experimental study of the partitioning of siderophile elements in a crystallizing lunar magma ocean. *Meteoritics & Planetary Science* 50:733–758.
- Siebert J., Corgne A., and Ryerson F. J. 2011. Systematics of metal–silicate partitioning for many siderophile elements applied to Earth's core formation. *Geochimica et Cosmochimica Acta* 75:1451–1489.
- Siebert J., Badro J., Antonangel D., and Ryerson F. J. 2013. Terrestrial accretion under oxidizing conditions. *Science* 339:1194–1197.
- Simon J. I. and DePaolo D. J. 2010. Stable calcium isotopic composition of meteorites and rocky planets. *Earth and Planetary Science Letters* 289:457–466.
- Smith M. R., Laul J. C., Ma M.-S., Huston T., Verkoeteren R. M., Lipschutz M. E., and Schmitt R. A. 1984. Petrogenesis of the SNC (shergottites, nakhlites, chassignites) meteorites: Implications for the origin from a large, dynamic planet, possibly Mars. *Proceedings, 14th Lunar and Planetary Science Conference, Journal of Geophysical Research* 89:B612–B630.
- Snyder D. A. and Carmichael I. S. E. 1992. Olivine-liquid equilibria and the chemical activities of FeO, NiO, Fe<sub>2</sub>O<sub>3</sub>, and MgO in natural basic melts. *Geochimica et Cosmochimica Acta* 56:303–318.
- Sutton S. R., Karner J., Papike J., Delaney J. S., Shearer C., Newville M., and Dyar M. D. 2005. Vanadium K edge XANES of synthetic and natural basaltic glasses and application to microscale oxygen barometry. *Geochimica et Cosmochimica Acta* 69:2333–2348.
- Suzuki T. and Akaogi M. 1995. Element partitioning between olivine and silicate melt under high pressure. *Physics and Chemistry of Minerals* 22:411–418.
- Taylor G. J. 2013. The bulk composition of Mars. *Chemie Der Erde-Geochemistry* 73:401–420.
- Taylor G. J. and Wieczorek M. A. 2014. Lunar bulk chemical composition: A post-Gravity Recovery and Interior Laboratory reassessment. *Philosophical Transactions of the Royal Society of London A: Mathematical, Physical and Engineering Sciences* 372:20130242.
- Taylor S. R. 1982. *Planetary science: A lunar perspective*. Houston, Texas: Lunar and Planetary Institute, LPI Publication No. 3303, 431 p.
- Taylor S. R., Rudowski R., Muir P., Graham A., and Kaye M. 1971. Trace element chemistry of lunar samples from the Ocean of Storms. *Proceedings, 2nd Lunar Science Conference*. pp. 1083–1099.
- Van Acherbergh E., Ryan C. G., and Griffin W. L. 1999. GLITTER: On-line interactive data reduction for the laser ablation inductively coupled plasma mass spectrometry microprobe. In *Ninth Annual VM Goldschmidt Conference*.
- Wade J. and Wood B. J. 2005. Core formation and the oxidation state of the Earth. *Earth and Planetary Science Letters* 236:78–95.
- Wang M.-S., Mokos J. A., and Lipschutz M. E. 1999. Martian meteorites: Volatile trace elements and cluster analysis. *Meteoritics & Planetary Science* 33:671–675.
- Wang Z., Laurenz V., Petitgirard S., and Becker H. 2016. Earth's moderately volatile element composition may not be chondritic: Evidence from In, Cd and Zn. *Earth and Planetary Science Letters* 435:136–146.
- Wänke H. and Dreibus G. 1986. Geochemical evidence for the formation of the Moon by impact-induced fission of the proto-Earth. In *Origin of the Moon*, edited by Hartmann W. K., Phillips R. J., and Taylor G. J. Houston, Texas: Lunar and Planetary Institute. pp. 649–671.
- Wänke H., Rieder R., Baddenhausen H., Spettel B., Teschke F., Quijanorico M., and Balacescu A. 1970. Major and trace elements in lunar material. *Proceedings, Apollo 11th Lunar Science Conference*. pp. 1719–1736.
- Wänke H., Wlotzka F., Baddenhausen H., Balacescu A., Spettel B., Teschke F., Jagoutz E., Kruse H., Quijano-

- Rico M., and Rieder R. 1971. Apollo 12 samples: Chemical composition and its relation to sample locations and exposure ages, the two-component origin of the various soil samples and studies on lunar metallic particles. Proceedings, 2nd Lunar Science Conference. pp. 1187–1199.
- Wänke H., Baddenhausen H., Balacescu A., Teschke F., Spettel B., Dreibus G., Palme H., Quijano-Rico M., Kruse H., Wlotzka F., and Begemann F. 1972. Multi-element analyses of lunar samples and some implications of the results. Proceedings, 3rd Lunar Science Conference. pp. 1251–1268.
- Wänke H., Baddenhausen H., Dreibus G., Jagoutz E., Kruse H., Palme H., Spettel B., and Teschke F. 1973. Multi-element analyses of Apollo 15, 16 and 17 samples and the bulk composition of the Moon. Proceedings, 4th Lunar Science Conference. pp. 1461–1481.
- Warren P. H. 2005. “New” lunar meteorites: Implications for composition of the global lunar surface, lunar crust, and the bulk Moon. *Meteoritics & Planetary Science* 40:477–506.
- Warren P. H., Kallemeyn G. W., and Kyte F. T. 1999. Origin of planetary cores: Evidence from highly siderophile elements in Martian meteorites. *Geochimica et Cosmochimica Acta* 63:2105–2122.
- Wing B. A. and Farquhar J. 2015. Sulfur isotope homogeneity of lunar mare basalts. *Geochimica et Cosmochimica Acta* 170:266–280.
- Witt-Eickschen G., Palme H., O’Neill H. S. C., and Allen C. M. 2009. The geochemistry of the volatile trace elements As, Cd, Ga, In and Sn in the Earth’s mantle: New evidence from in situ analyses of mantle xenoliths. *Geochimica et Cosmochimica Acta* 73:1755–1778.
- Wolf R., Woodrow A., and Anders E. 1979. Lunar basalts and pristine highland rocks—Comparison of siderophile and volatile elements. Proceedings, 10th Lunar and Planetary Science Conference. pp. 2107–2130.
- Wombacher F., Rehkämper M., Mezger K., and Münker C. 2003. Stable isotope compositions of cadmium in geological materials and meteorites determined by multiple-collector ICPMS. *Geochimica et Cosmochimica Acta* 67:4639–4654.
- Wombacher F., Rehkämper M., Mezger K., Bischoff A., and Münker C. 2008. Cadmium stable isotope cosmochemistry. *Geochimica et Cosmochimica Acta* 72:646–667.
- Wood B. J., Kiseeva E. S., and Mirolo F. J. 2014. Accretion and core formation: The effects of sulfur on metal–silicate partition coefficients. *Geochimica et Cosmochimica Acta* 145:248–267.
- Yang S., Humayun M., Righter K., Jefferson G., Fields D., and Irving A. J. 2015. Siderophile and chalcophile element abundances in shergottites: Implications for Martian core formation. *Meteoritics & Planetary Science* 50:691–714.
- Yi W., Halliday A. N., Lee D. C., and Christensen J. N. 1995. Indium and tin in basalts, sulfides, and the mantle. *Geochimica et Cosmochimica Acta* 59:5081–5090.
- Yi W., Halliday A. N., Alt J. C., Lee D. C., Rehkämper M., Garcia M. O., and Su Y. 2000. Cadmium, indium, tin, tellurium, and sulfur in oceanic basalts: Implications for chalcophile element fractionation in the Earth. *Journal of Geophysical Research: Solid Earth* 105:18,927–18,948.
- Young E. D., Kohl I. E., Warren P. H., Rubie D. C., Jacobson S. A., and Morbidelli A. 2016. Oxygen isotopic evidence for vigorous mixing during the Moon-forming giant impact. *Science* 351:493–496.
- Zhang J., Dauphas N., Davis A. M., Leya I., and Fedkin A. 2012. The proto-Earth as a significant source of lunar material. *Nature Geoscience* 5:251–255.

## SUPPORTING INFORMATION

Additional supporting information may be found in the online version of this article:

**Table S1:** Comparison of standards analyzed as unknowns, utilized in LA-ICP-MS analysis at Rice and University of Houston (all measurements in ppm).